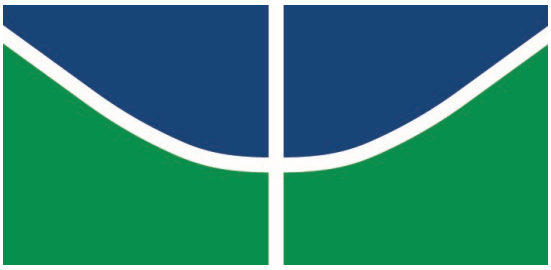

University of Brasília

Institute of Physics

Master's Dissertation

Structural and Electronic Properties of the Cove-type Graphene Nanoribbons

Tiago de Sousa Araújo Cassiano

Advisor: Prof. Pedro Henrique de Oliveira Neto

Tiago de Sousa Araújo Cassiano

Structural and Electronic Properties of the Cove-type Graphene Nanoribbons

Master's Dissertation presented to the Institute of Physics of the University of Brasília as a partial requirement to obtain the Master title

Advisor: Prof. Pedro Henrique de Oliveira Neto

Brasilia, July of 2021.

"I may not believe in myself, but I believe in what I’m doing."

James Patrick Page

Acknowledgements

To my mother, Lucenira de Sousa Araújo, and my aunt, Maria das Graças Aureliano, for their continuous support, caring, and understanding. This work would not be possible without you two. Thanks for, even not knowing what I do, still believe in my effort.

To Larissa dos Santos Born, for being an immeasurable source of kindness, companionship, and joy. Thanks for daily softening all the difficulties and intensifying all the achievements.

To all the incredible teachers which I had the pleasure to be guided by during this period. My advisor, Pedro Henrique Oliveira Neto, for the endless effort in tutoring and develop my scientific and personal formation. Professor Geraldo Magela, for the exciting lectures, the patience, and the rich discussions. Professor Ricardo Gargano, for the pleasant encounters and conversations.

To the members of my group. Dr. Leonardo Evaristo de Sousa, for the guidance, the tolerance, and the enthusiasm in our endeavors. Fernando Teixeira Bueno, and Israel Siqueira, for the funny discussions and friendship. To Jacyara Flores Arbues Carneiro, my office neighbor. To them, and to those who were not mentioned, thank you for the laughter, work, and frustration shared.

To all my friends, from the institute or not, thank you for the support and the moments of joy and work shared.

Resumo

Nos últimos anos, o grafeno vem promovendo inúmeros avanços tecnológicos e científicos. Entretanto, o material não apresenta um valor de *bandgap* diferente de zero. Por isso, a aplicação de grafeno puro em dispositivos semicondutores é inviável. Uma possível alternativa reside na produção de nanofitas de grafeno, ou *graphene nanoribbons* (GNR) em inglês. Nesse sentido, um estudo recente descreve a síntese de uma geometria inédita de GNR. Conhecida como, *cove-type* GNR, ou CGNR, essa molécula apresenta diversas propriedades em sua síntese que indicam um potencial uso em produção industrial. Todavia, pouco se sabe das potencialidades em conduzir mudanças em sua rede. Neste trabalho, investigamos as propriedades estruturais e eletrônicas ao conduzir dois tipos de transformações: aumento de largura e variação da distância entre os anéis de borda (λ). O estudo será feito através de simulações computacionais com base no modelo Su-Schrieffer-Heeger (SSH) bi-dimensional estendido, com acoplamento elétron-fónon. Resultados mostram que o CGNR permite uma calibração suave e monotônica no gap, seja mudando a sua largura, ou λ. Tal propriedade, não observada em nanofitas ordinárias até então, indica um potêncial latente superior. O trabalho também aborda as caracteristicas das redes associadas com cada transformação. Os resultados mostram que o CGNR é um forte candidato a ser tornar um material base na optoeletrônica no futuro.

Abstract

Over the past years, graphene is driving numerous theoretical and technological breakthroughs. However, it presents no bandgap. Because of that, the use of graphene in semiconductor applications is diminished. An alternative is to rely on the so-called graphene nanoribbons (GNRs). In that sense, a recent study described a new GNR type, known as cove-type GNR (CGNR), with a synthesis route suitable for large-scale production. Still, little is known about the potential in modifying CGNR's lattice. In this work, we investigated the structural and electronic properties in change the CGNR lattice by two transformations: changes in the width and the distance between the uppermost rings in the edge (λ). The study will unravel through computational simulations using the 2-D extended Su-Schrieffer-Heeger (SSH) model with electron-phonon constant. Results show that the CGNR can endure a monotonic gap decay tuning process by varying the width or λ. Such attribute was not observable in other GNRs so far. This study also discusses the lattice's characteristics associated with each transformation. In conclusion, the results show that the CGNR is a strong candidate to become a fundamental material in future optoelectronics.

CONTENTS

CHAPTER 1

INTRODUCTION

1.1 Graphene

Since its isolation in 2004 [1], graphene is displaying boundless potential in materials science. Much of the attention regarding this one-atom-thick carbon allotrope lies on its unique physicochemical properties [2, 3]. Among other facets, its mechanical, optical, and thermal [4, 5] responses have special relevance. Unlike many other organic materials, graphene is able to endure intense mechanical stress [6] while being extremely light-weighted. In addition, this transparent material [7, 8] can efficiently conduct heat at wide temperature regimes [9]. Besides, the electronic properties are even more promising. Unlike any other material in nature, graphene presents a linear band structure [10]. This attribute allows, at least theoretically, massless charge carriers. As a consequence, charge transport in graphene is incredibly favored. This material can potentially change fundamental aspects of our society and current state technology.

Compared with other carbon allotropes, graphene-oriented research is relatively new. Regardless, its applicability already branches many fields. Currently, there are reports of engi-

neering efforts based on its mechanical proprieties [11, 12], the development of sensing devices [13], biomedical solutions [14], and especially electronic apparatus [15, 16, 17].

Besides all prospects, graphene is a semi-metal, having no bandgap [10]. This property greatly limits its use in nanoelectronics. Currently, there are several techniques focused on opening the gap. Among them, two procedures have special relevance. The doping approach [18] consists of inserting non-carbon atoms in the lattice. This structural change enforces a symmetry break, giving rise to a non-zero gap. In most cases, the elements chosen are oxygen, nitrogen, or boron. The inclusion of each doping constituent can tailor the material towards specific applications [19]. At this moment, doping is promoting the development of diverse applications in electrochemical energy storage [20, 21], gas and optical sensing [22, 23], and photovoltaics [24]. However, the strategy bears limitations. Some syntheses rely on the grafting process, which inevitably depletes the mobility [25].

1.2 Graphene nanoribbons (GNRs)

The electronic confinement offers a more elegant way to open the gap by shaping the lattice into nanoribbons. The so-called graphene nanoribbons (GNRs) [26, 27, 28] are quasi-one-dimensional nanoestructures that provide a strong alternative for future optoelectronics. Being a derivative of graphene, GNRs share many characteristics with its parent-material [29]. Among others, the nanoribbons present high mechanical strength [30], high charge mobility [31, 32] and favorable thermal properties [33]. Besides, GNRs have an ultrahigh surface area [34, 29] and the possibility of tuning its electronic properties [35, 36, 37]. The latter attribute

allows highly customized materials, opening a wide range of design possibilities as well as applicability.

1.2.1 Some Types

The electronic response of a GNR is mainly dictated by its edge shape. Nanoribbons with different edges might display entirely distinct properties. There are three main classes, armchair (AGNR), zig-zag (ZGNR), and chiral (chGNR). Each one refers to a different length axis. Figure 1.1 illustrates all edge shape classes along their respective axes. The diversity inside each class is growing every day through the emerging sub-classes.

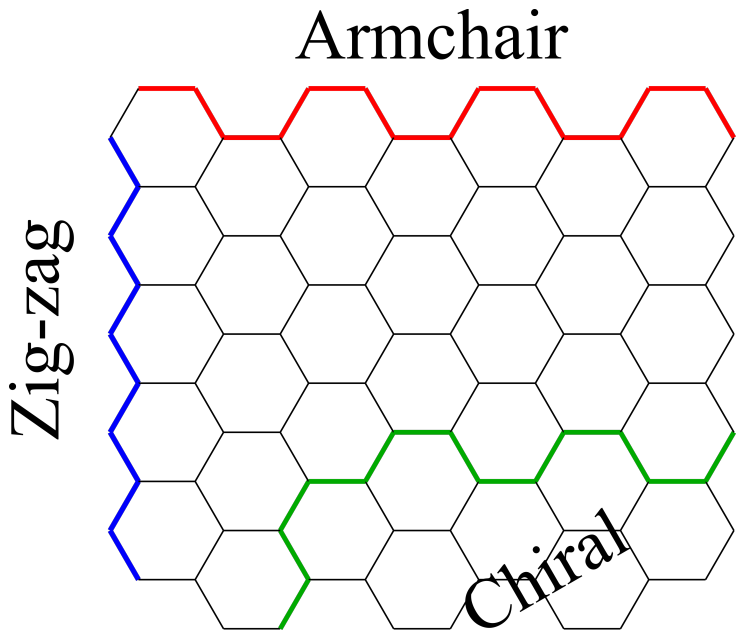

Figure 1.1: Schematic illustration of the three main GNR's classes: armchair (red), zig-zag (blue) and chiral (green). Each type branches in several sub-classes geometries, which display widely distinct physical properties.

Armchair Graphene Nanoribbons (AGNRs)

The armchair class is a type of GNR with edges resembling an armchair. It is one of the first synthesized GNRs. Currently, most of the effort concentrates on investigating this nanoribbon. Its pure form has three width families, 3N, 3N+1, and 3N+2, where N is the number of sites along the width axis [26, 28]. AGNRs that belong to families 3N and 3N+1 have an appreciable gap. Inversely, the specimens in the 3N+2 family behave as semi-metals. By far, the AGNR type is the one with the most number of sub-classes. Here we mention the chevron [38, 39], and the heterojunctions [40].

Zig-zag Graphene Nanoribbons (ZGNRs)

Unlike AGNRs, pure zig-zag nanoribbons do not group up in width families. Regardless of the width size, these materials behave as semi-metals. Although this attribute diminishes the applicability in optoelectronics, ZGNRs have an important role in others fields, such as spintronics [41, 42]. However, it is worth mention that, just like in graphene, doping ZGNRs allows its use in semiconducting applications [43].

Interestingly, the ZGNR contains a subclass of nanoribbons with a finite gap. Firstly synthesized in 2014, they are known as cove-type graphene nanoribbons (CGNR) [44, 31]. The chemical diagrams of some CGNRs are illustrated in figure 1.2. Just like in AGNRs, the CGNRs have specimens with different widths. Throughout this work, we will label them as N-CGNR, where N is the number of carbon sites along the width axis. Besides the energy bandgap, the reports indicate the existence of superior attributes in both production and performance. The synthesis is a liquid-based bottom-up process. That means that the material arises from smaller

chemical precursors and supports large-scale production. Consequently, the specimens have almost no defects. Besides the high quality, the nanoribbon is unusually long, extending up to 200 nm. All these attributes strengthen the potential of this sub-class. Therefore, studying such material can impact both theoretical and technological fields of low-dimensional organic semiconductors.

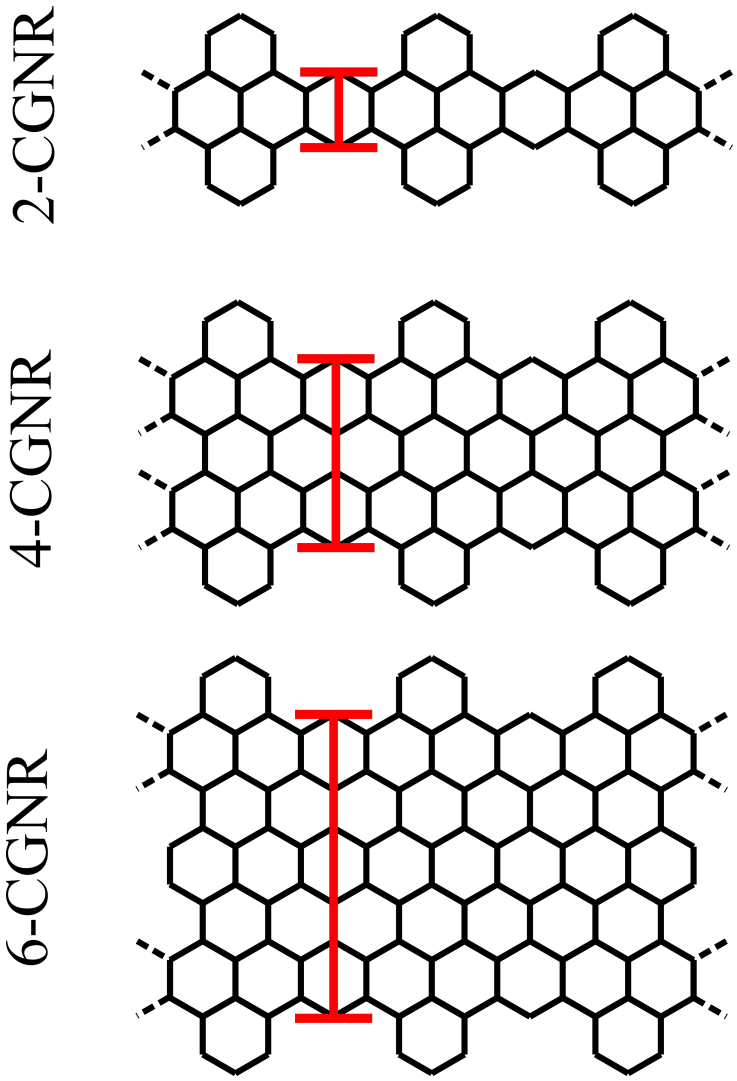

Figure 1.2: Chemical diagram of CGNRs with different width sizes. Throughout this work, we are going to follow the labeling convention of this figure.

Regarding the physical properties, CGNRs also deliver promising results. UV-vis spec-

trum reveals an optical gap of 1.88 eV. This is an adequate value for electronics [28]. Moreover, terahertz spectroscopy measurements point out an unusually high intramolecular mobility in CGNRs of up to $15\,000\,\mathrm{cm}^2/\mathrm{Vs}$ [31]. This outstanding value, almost 10 % of pure graphene's mobility [45, 46], has no comparable counterpart among the semiconducting GNRs. These properties reinforce the potential around the CGNRs and justify further investigation of its electronic nature.

Chiral Graphene Nanoribbons (chGNRs)

The chiral border is a convolution of segments from the previous classes. Different chGNR specimens are often classified by the angle between their edges and the zig-zag axis [47]. These materials have a characteristic low bandgap due to a high degree of aromaticity and an electron delocalization [29, 48]. Besides, controlling the proportion of each segment has proven to be a potential strategy for fine-tuning designs [49].

1.3 Applicability of GNRs

The participation of GNRs in technological applications is diverse. As stated earlier, the edge shape plays a definitive role in the ultimate electronic, mechanical and thermal properties. For that reason, different GNRs often are suitable to perform entirely distinct tasks. Here, we emphasize two prominent fields: optoelectronics and bio-medicine.

1.3.1 Optoelectronics

In optoelectronics, organic semiconductors have an important role in almost any potential device. In the case of GNR, its use in organic field-effect transistors (OFETs) presents formidable prospects. The atomically thin body, possibility of gap modularization, and the high on-current density of semiconducting AGNRs turn them into candidates for ultra-scaled FETs [50, 51]. Experimental measurements show that, on many definitive properties, GNR-based OFETS overcome state-of-the-art technologies [51]. Moreover, unlike their current counterparts, nanoribbons can endure intense mechanical stress, as stated earlier. This feature allows the production of flexible electronic components for wearable applications [29, 51, 52]. Furthermore, others devices integrate GNRs in gas sensing [53, 54] and in photovoltaic cells [55, 56].

1.3.2 Biomedical Devices

The versatility of GNR's geometries permits the use in diagnosis, treatment, and research on several biomedical fields. Most of the effort is focused on biosensing-oriented devices [29]. Recent reports indicate the possibility of using GNRs to detect many biological markers, such as glucose [57, 58], DNA [59], and amino acids [60]. Biosensing strategies are also employed in cancer therapy, as an effective monitoring tool [61]. The incredible surface area also permits use in other applications like drug delivery and photothermal therapy [62].

1.4 Objective

Considering the latent potential of the CGNR, we propose to investigate this material employing a theoretical model known as the SSH model. The study evaluates the physical consequences of performing a unique border transformation. The project's specific objectives can be summarized in:

1. Evaluate the gap response due to the edge change;

2. Investigate the effects in the lattice as the design strategy is enforced;

3. Identify the technique's potential when compared with other established gap-changing structure strategies.

The text is organized into three chapters. Chapter 1 delivers a broad introduction to the GNRs and their place in materials science. Next, chapter 2 develops the theoretical background needed to simulate GNRs in the SSH model framework. Finally, chapter 3 addresses the study of edge changes in the CGNR as a gap-tuning strategy.

CHAPTER 2

THEORETICAL MODELING

Atomic species with sp^2 hybridization present three orbitals arranged in a plane and one p_z-type perpendicular to them. The overlapping of the planar atomic orbitals creates the σ-orbitals. In the same fashion, π-orbitals emerge from the superposition of two neighboring orbitals perpendicular to the plane. Electrons that occupy σ orbitals are related with stronger bonds than the ones in π. As a result, materials that exhibit such hybridization through its entire extension have a valence band with fully occupied σ orbitals and half-filling π orbitals. Moreover, the π-electrons become delocalized. A precise physical description of such systems would require the accountability of each electron. Unfortunately, this restriction turns the approach impracticable to large systems such as linear polymers or graphene.

As an alternative, we can rely in simple model Hamiltonians which, although requiring strong approximations, preserve the system's fundamental characteristics. Here we initially as-

sume two simplifications. The first one is to restrict the physical description only to low-energy excitations. By doing that, the electronic description will be mediated only by π-electrons. The second approximation is to ignore any long-range electron hopping, while using the a linear combination of atomic orbitals as basis. The combination of these two assumptions can be accommodated in the tight-binding (TB) model.

However, in spite of its undeniable importance in quantum chemistry, the pure TB model is not suitable to simulate extended organic π-conjugated systems, such as the poly-acetylene [63]. Such limitation encouraged Su, Schrieffer and Heeger to come up with an better modeling that would be later known as the Su-Schrieffer-Heeger (SSH) model [63, 64]. Here, we are going to use this development to investigate the GNRs. Historically, the formalism was initially applied to a simple system: the linear polymer. We chose to start our development in the same ground. Gradual enhancements are carried out until an adequate description for graphene-based materials arise.

2.1 1-D Generalized Hamiltonian for a Chain via SSH model

Under the approximations regarding the SSH model, the Hamiltonian of a chain follows [63, 65, 66, 64]:

$$H = H_{tb} + H_{lattice}. \tag{2.1}$$

Here, H_{tb} is the Hamiltonian term representing the electronic description mediated by the π-electrons, grounded in the tight-binding model, while $H_{lattice}$ accounts for the inter-site

lattice interaction. As stated before, the model assumes a low-energy regime. Consequently, the amplitude of the lattice movement should be modest. Past works corroborate this assumption [67]. Under reasonable conditions, conjugated polymers have lattice distortions around 3% around the equilibrium bond length [68]. Similar behavior is shared with graphene-based systems. This setting encourages us to model the lattice phenomena under a simple harmonic approximation. Let u_n be the relative position of the n-th site with respect to its undistorted position, as depicted in figure 2.1, then

$$H_{lattice} = \frac{1}{2}\sum_n M\dot{u_n}^2 + \sum_n \frac{K}{2}(u_{n+1} - u_n)^2. \tag{2.2}$$

The first term accounts for the kinetic part, while the latter is the potential one. M and K are the site mass and the Hook's constant, respectively.

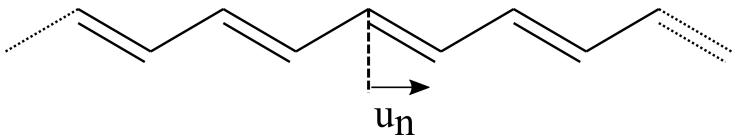

Figure 2.1: Chemical diagram of the polyacetylene, a representative of the linear polymers. The variable u_n represents the relative position of the n-th site.

As mentioned before, the SSH assumption considers only the hopping between first neighbors. Therefore, H_{tb} in the second quantization formalism reads

$$H_{tb} = -\sum_{n,s} t_{n+1,n}(C^\dagger_{n+1,s}C_{n,s} + C^\dagger_{n,s}C_{n+1,s}), \tag{2.3}$$

in which $C^\dagger_{n+1,s}$ is the creation operator. Thus, its application creates a π-electron in the $n+1$-th site with spin s. Accordingly, $C_{n,s}$ is the destruction operator. When acted in a given state, this

operator annihilates a π-electron with spin s from the n-th site. $t_{n+1,n}$ is the so-called hopping integral. It is associated with the amplitude probability of a π electron jump. Early developments treated $t_{n+1,n}$ as a constant regardless of the lattice spatial displacement. For some systems, such approximation produces good results. However, as it is well known, transport in graphene-based materials has a paramount influence of quasiparticles [69, 70, 71, 72]. These individuals rise from the interplay of the electronic and lattice phenomena. Therefore, refinement of the hopping integral is a mandatory step to simulate more complex systems.

2.1.1 Electron-phonon Coupling Inclusion

There is not an analytical way to determine $t_{n+1,n}$. However, it is possible to find an approximated expression based on the type of system considered [73]. As stated before, the distance between sites in conjugated polymers and graphene-based materials oscillate modestly around the undistorted bond length value. Therefore, we are inclined to expand $t_{n+1,n}$ around this reference distance [64]. In other words:

$$t_{n+1,n} = t_0 - \alpha(u_{n+1} - u_n). \tag{2.4}$$

α is the electron-phonon coupling constant [67, 74]. As the name suggests, it dictates the lattice influence over the electronic phenomena (and vice-versa). Each material presents a distinct response. Therefore, α must be evaluated individually for every system. In this work, we carried a tuning procedure based on the optical bandgap. The method is described in section 3.2.1.

Here, we emphasize that the expected qualitative behavior holds. Given two adjacent sites, $t_{n+1,n}$ must decrease as the inter-site distance grows. This is so because the more distant the sites are, the weaker the overlap between their p_z orbitals will be. Thus, the hopping becomes more difficult. In that sense, shrinking the distance must cause the inverse effect: an increase in hopping rates. Furthermore, $t_{n+1,n}$ must return to a constant value (t_0) in the absence of distortions.

2.1.2 Solving the Electronic Hamiltonian

We initiate the solving procedure by the stationary case. For now, any site motion will be discarded. Therefore,

$$\dot{u_n} = 0 \quad \forall n. \tag{2.5}$$

This condition translates into

$$H = -\sum_{n,s} t_{n+1,n}(C^{\dagger}_{n+1,s}C_{n,s} + C^{\dagger}_{n,s}C_{n+1,s}) + \sum_{n} \frac{K}{2}(u_{n+1} - u_n)^2. \tag{2.6}$$

Our objective is to diagonalize this operator. Because the Hamiltonian does not present any term that couples electrons with a different spin, we can carry the diagonalization separately for each spin s. Suppose that $\{a_{k,s}\}$ are the diagonalizing operators. Then,

$$H = \sum_{k,s} E_{k,s} a^{\dagger}_{k,s} a_{k,s}. \tag{2.7}$$

In order to explicitly find the diagonal form of Eq. 2.7 we must relate $\{C_{n,s}\}$ and $\{a_{k,s}\}$. This is done by introducing a transformation such that

$$\begin{aligned} a_{k,s} &= \sum_n b_{nks} C_{n,s}, \\ a^\dagger_{k,s} &= \sum_n b^*_{nks} C^\dagger_{n,s}. \end{aligned} \tag{2.8}$$

The coefficients must preserve probability. This forces us to also enforce unitary. Then, for every eigenstate set with spin s,

$$\mathbf{b}^\dagger \mathbf{b} = \mathbf{1}, \tag{2.9}$$

where each element in $\mathbf{1}$ holds, individually,

$$\begin{aligned} \mathbf{1}_{n'n} &= \sum_k (\mathbf{b})_{n'k} (\mathbf{b}^\dagger)_{kn} = \sum_k (\mathbf{b})^*_{nk} (\mathbf{b})_{n'k} = \delta_{n'n}, \\ \mathbf{1}_{k'k} &= \sum_n (\mathbf{b}^\dagger)_{k'n} (\mathbf{b})_{nk} = \sum_n (\mathbf{b})^*_{nk'} (\mathbf{b})_{nk} = \delta_{k'k}. \end{aligned} \tag{2.10}$$

Using these relations permit reverse Equation 2.8, leading to:

$$\begin{aligned} C_{n,s} &= \sum_k b^*_{nks} a_{k,s}, \\ C^\dagger_{n,s} &= \sum_k b_{nks} a^\dagger_{k,s}. \end{aligned} \tag{2.11}$$

Substitution in Eq. 2.6 gives

$$\begin{aligned} H_{ele} &= -\sum_{n,s}\sum_{k,k'}[t_{n+1,n}b_{n+1ks}b^{*}_{nk's} + t^{*}_{n+1,n}b_{nks}b^{*}_{n+1k's}]a^{\dagger}_{k,s}a_{k',s} \\ &= \sum_{k,s} E_{k,s}a^{\dagger}_{k,s}a_{k',s} = \sum_{k,k',s} E_{k,s}\delta_{k,k'}a^{\dagger}_{k,s}a_{k',s} \end{aligned} \tag{2.12}$$

After reordering the summation indices and inserting $\mathbf{1}$ in the last equation, we get

$$-t_{n+1,n}b_{n+1ks} - t^{*}_{n,n-1}b_{n-1ks} = E_{ks}b_{nks}. \tag{2.13}$$

The boundary terms require special care. Enforcing a periodic boundary relationship leads to

$$\begin{aligned} t_{0,n} &= t_{N,n}, \\ t_{N+1,n} &= t_{1,n}, \\ t_{n,0} &= t_{n,N}, \\ t_{n,N+1} &= t_{n,1}. \end{aligned} \tag{2.14}$$

Now, we are able to write the electronic Hamiltonian in matrix notation. Combining Eq. 2.13

and 2.14 we have, for each spin s,

$$\begin{bmatrix} 0 & t_{2,1} & 0 & \cdots & t^*_{1,N} \\ t^*_{2,1} & 0 & t_{3,2} & \cdots & 0 \\ 0 & t^*_{3,2} & 0 & \cdots & 0 \\ \vdots & & & \ddots & \\ t_{1,N} & 0 & \cdots & t^*_{N,N-1} & 0 \end{bmatrix} \begin{bmatrix} b_{1ks} \\ b_{2ks} \\ b_{3ks} \\ \vdots \\ b_{Nks} \end{bmatrix} = E_{ks} \begin{bmatrix} b_{1ks} \\ b_{2ks} \\ b_{3ks} \\ \vdots \\ b_{Nks} \end{bmatrix}. \tag{2.15}$$

2.1.3 Solving Lattice

In principle, the only task that remains is to diagonalize the matrix in Eq. 2.15. However, we recall Eq. 2.4. Each hopping term will depend on the site's spatial coordinates. Therefore, in other words, to numerically evaluate the matrix requires knowledge of the stationary state from the start. We can crack this apparent loophole by solving the lattice first.

In view of the Ehrenfest theorem [75], the Euler-Lagrange equations with respect to the relative displacement $\{u_i\}$ must hold when calculated with expected the value of the Lagrangian ($\langle L \rangle$) [71, 76]. Then,

$$\frac{d}{dt}\left(\frac{\partial \langle L \rangle}{\partial \dot{u}_i}\right) = \frac{\partial \langle L \rangle}{\partial u_i}, \tag{2.16}$$

for a given state $|\psi\rangle$. Here we choose a Slater determinant composed of the occupied orbitals from the diagonalizing ($\{a_k\}$) basis. In other words,

$$|\psi\rangle = |1, 2, \cdots, N\rangle = a_1^\dagger a_2^\dagger \cdots a_N^\dagger \,|\quad\rangle\,. \tag{2.17}$$

Let V and T be, respectively, the expected value of the potential and kinetic energy. Recalling the stationary approximation, we have

$$\begin{aligned}
\langle L\rangle &= \langle T\rangle - \langle V\rangle = -\langle V\rangle\,, \\
\langle L\rangle &= \langle\psi|\left[\sum_{n,s} t_{n+1,n}(C^{\dagger}_{n+1}C_n + C^{\dagger}_{n}C_{n+1}) - \sum_n \frac{K}{2}(\eta_n)^2\right]|\psi\rangle\,, \\
\langle L\rangle &= \sum_{n,s} t_{n+1,n}(\langle C^{\dagger}_{n+1}C_n\rangle + \langle C^{\dagger}_{n}C_{n+1}\rangle) - \sum_n \frac{K}{2}(\eta_n)^2.
\end{aligned} \tag{2.18}$$

Where, for convenience, we label $\eta_i = u_{i+1} - u_i$. From Eq. 2.11 and 2.17

$$\begin{aligned}
\sum_s \langle C^{\dagger}_{n+1,s}C_{n,s}\rangle &= \langle\psi|\sum_{k,k',s} b_{n+1ks}b^{*}_{nk's}a^{\dagger}_{k,s}a_{k',s}\,|\psi\rangle\,, \\
&= \sum_{k,k',s} b_{n+1ks}b^{*}_{nk's}\,\langle\quad|\,a_1\cdots a_N(a^{\dagger}_{k,s}a_{k',s})a^{\dagger}_1\cdots a^{\dagger}_N\,|\quad\rangle\,, \\
&= \sum_{k,s}{}' b_{n+1ks}b^{*}_{nks} \equiv B_{n+1n},
\end{aligned} \tag{2.19}$$

in which the prime sign indicates a summation over only the occupied orbitals. Then, rewriting $\langle L\rangle$ with this new notation gives

$$\begin{aligned}
\langle L\rangle &= \sum_n t_{n+1n}(B_{n+1n} + B^{*}_{n+1n}) - \sum_n \frac{K}{2}(u_{n+1} - u_n)^2, \\
&= \sum_n (t_0 - \alpha\eta_n)(B_{n+1n} + B^{*}_{n+1n}) - \sum_n \frac{K}{2}(\eta_n)^2.
\end{aligned} \tag{2.20}$$

Taking the derivative of $\langle L\rangle$ with respect to an arbitrary $\eta_{n'}$, and carrying out the sums leads to

$$\frac{\partial\langle L\rangle}{\partial\eta_{n'}} = -\alpha(B_{n'+1n'} + B^{*}_{n'+1n'}) - K\eta_{n'}. \tag{2.21}$$

Since we are in the stationary case [72, 71],

$$\frac{d}{dt}\left(\frac{\partial \langle L \rangle}{\partial \dot{\eta}_{n'}}\right) = 0, \tag{2.22}$$

leading to

$$K\eta_n = -\alpha(B_{n+1n} + B^*_{n+1n}). \tag{2.23}$$

2.1.4 Stationary Algorithm

Eq. 2.23 relates the lattice and the electronic parts apart from the Schrodinger equation. Now, we are able to find a set of $\{\eta\}$ to be used in the Hamiltonian of Eq. 2.15. With that, the electronic part can be solved through the lattice and vice-versa. The self-consistent algorithm can be summarized by the following steps:

1. Guess a set of $\{\eta\}$;
2. Build the electronic Hamiltonian of Eq. 2.15;
3. Diagonalize Eq. 2.15;
4. Calculate the $\{B_{n+1n}\}$;
5. Find a new set of $\{\eta_{new}\}$ via Eq. 2.23;
6. Under a convergence criterion, $\{\eta_{new}\}$ is equal to $\{\eta\}$?
    - If so, returns $\{\eta_{new}\}$ and the $\{b_{k,s}\}$ as the stationary configuration;
    - If not, go back to step 1. using $\{\eta_{new}\}$ as the initial guess.

2.2 Generalization for 2-D Systems

Up to this point, all theoretical development described refers to one-dimensional polymer chains. We now focus on adapting the preceding theory to two dimensional systems. In order to do that, we must rewrite the Hamiltonian in Equation 2.1 considering the new lattice profile. Unlike on the 1-D case, now each site may have up to three first neighbors. As a consequence, the Hamiltonian turns into [71, 77, 78, 37, 79]

$$H = -\sum_{<i,j>,s} (t_0 - \alpha\eta_{i,j})(C^{\dagger}_{i,s}C_{j,s} + h.c.) + \sum_i \frac{P_i^2}{2M} + \sum_{<i,j>} \frac{K}{2}\eta_{i,j}^2, \tag{2.24}$$

in which the index $< i, j >$ refers to sums over the first neighbors, as illustrated in Figure 2.2. Comparing with the one-dimensional case, the pair-wise sum is the only change. Then, all previous approaches are still suitable to this new operator. Not surprisingly, we are going to reapply the solving methods of the previous sections. All algorithms will remain valid, apart from changes in the expressions used.

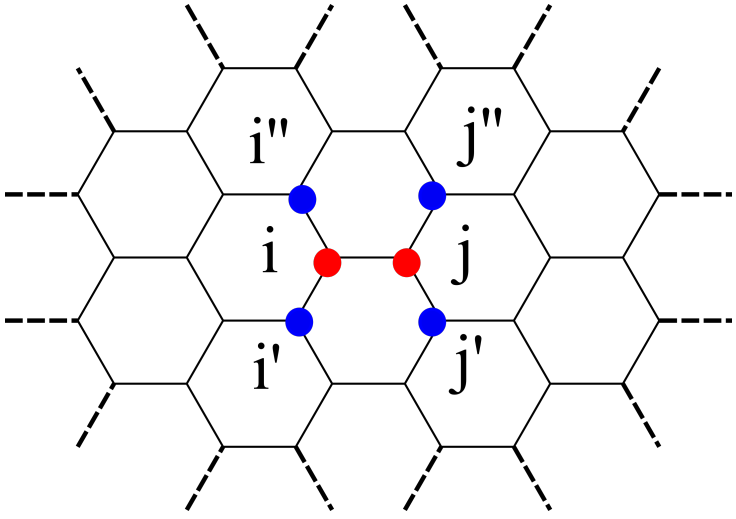

Figure 2.2: Index scheme used in the 2-D extension of the SSH Hamiltonian.

2.2.1 Stationary States

Recalling section 2.1.3, one must find the equations of motion of the generalized coordinates to obtain stationary states. In a analogous procedure that ends in the Eq. 2.23, we reach

$$\eta_{i,j} = -\frac{\alpha}{K}(B_{i,j} + h.c.), \tag{2.25}$$

where $B_{i,j}$ is defined according to Eq. 2.19. The solving procedure is analogous to the one described for one-dimensional chains.

CHAPTER 3

EDGE ENGINEERING IN COVE-TYPE GRAPHENE NANORIBBONS

3.1 The Problem

Physicists and chemists are on the hunt to extend the properties of the cove-shaped GNR [44] for future GNRs. This trend occurs because of the remarkable synthesis attributes involved in this nanoribbon. Recent procedures enabled the production of CGNRs with different widths via similar approaches. Now, as an additional step, one must find a way to explore one of the most pertinent features of the GNRs: the striking dependence between the edge shape and the physical properties [80]. Such a trait has a direct impact on future developing efforts. In optoelectronics, the material's usability depends on how easily its attributes can be mold, since industrial demands can be highly particular, requiring fine adjustments. In that sense, finding a precise way to tailor the physical properties of the CGNRs is a key task.

In most semiconductor-based devices, the energy bandgap is a decisive physical prop-

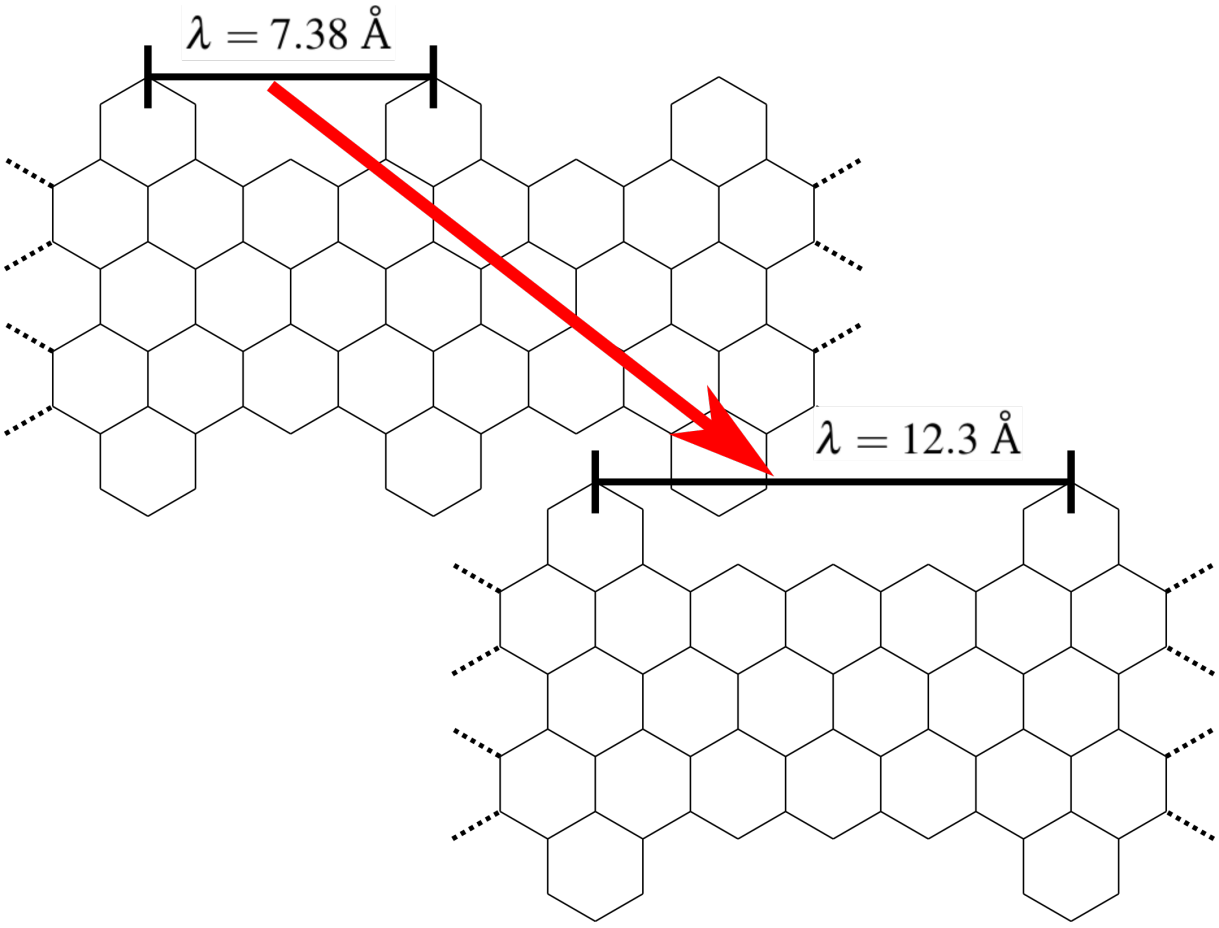

Figure 3.1: Illustration of the edge change strategy studied in this chapter. The approach consists in increasing the proportion of zig-zag chains in the original cove-type GNR [44] by varying parameter λ.

erty. Different applications often require distinct gap values. In that sense, modify a GNR's bandgap by simple edge changes impacts the applicability. As well documented in the literature, AGNRs allow gap tuning through width changes [26, 70]. However, this procedure leads to non-smooth gap variations. For instance, the energy difference between the bandgaps of 3-AGNR and 4-AGNR is 0.18 eV [26], while the same variation for the 4-AGNR and 5-AGNR is about 2 eV. This kind of sharp drop turns the process complex. Therefore, a smooth strategy to tune the energy bandgap can contribute to the inclusion of CGNRs in real applications.

A possible gap tuning route for CGNRs relies on an unique feature of its shape. Cove-

shaped edges arise from the superposition of AGNR's and ZGNR's borders. As well known, these two primordial GNRs may present opposite electronic properties [26, 28]. Because of that, varying the proportion of each edge-shape should affect GNR's gap. Figure 3.1 displays this strategy. Unlike the width change approach, such a simple edge change does not alter the nanoribbon's quantum confinement degree. Therefore, it would likely drive minor disturbances at the electronic properties. All the potential aside, this tuning strategy was not tested, until now.

In this chapter, we present the results regarding the investigation of the aforementioned edge change strategy in cove-type GNRs. Firstly, we estimate 4-CGNR's α through a semi-empirical approach. Then, the stationary algorithm is applied to CGNRs with different zig-zag chain extensions. Each simulated specimen had its bandgap evaluated. In this study, we considered four CGNRs types: 2-CGNR, 4-CGNR, 6-CGNR, and 8-CGNR. Results show a smooth monotonic gap decay due to the increasing of zig-zag edges proportion. This declining trend allows to smoothly reach band gaps between 0 eV to almost 3 eV. Also, we describe in detail the effects of this approach on CGNR's lattice. We observed that changing the proportion of AGNR and ZGNR on the cove-edge modifies the conjugation rate. As a direct response, the bond length distribution becomes significantly more disperse, translating into a morphological spreading. The corresponding published paper of this work is located in the appendix section 4.

3.2 Results

3.2.1 α-tuning

Estimating the electron-phonon coupling is a mandatory step to model GNRs over the described SSH Hamiltonian model. However, one can not directly determine it [73]. Each nanoribbon displays a distinct lattice-electronic response due to its shape. Thus, different specimens might possess a unique α. This limitation obliges us to use a tuning procedure. In other words, the optimal α will be the one that best reproduces some reliable electronic measure. Here, we choose the optical bandgap as this experimental reference. Figure 3.2(a) shows the energy bandgap as a function of α. Reports indicate that 4-CGNR has a gap of 1.88 eV [44]. Consequently, the correspondent α value is 4.6 eV/Å. Similar measurements for AGNRs found α around 3.5 and 5.5 eV/Å [81], indicating that both GNRs types might present akin lattice-electronic coupling.

Beyond α estimation, the profile of electronic energy states can effectively characterize quantum-confined materials [82, 66]. Figure 3.2(b) depicts this graph for the 4-CGNR. The set of lines below 0 eV represents the valence band, while the one above 0 eV is known as the conduction band. The energy shift between the highest occupied molecular orbital (HOMO) and the lowest unoccupied molecular orbital (LUMO) is the optical bandgap of 1.88 eV. The correspondent density of states (DOS) plot is located on the right side of Figure 3.2(b). Here, each energy state contributes to the distribution. The overall DOS behavior relates to other quantum confined materials. No π-electron can access the region delimited by HOMO and LUMO orbitals. That happens because cove-shaped edges provoke a lattice symmetry break,

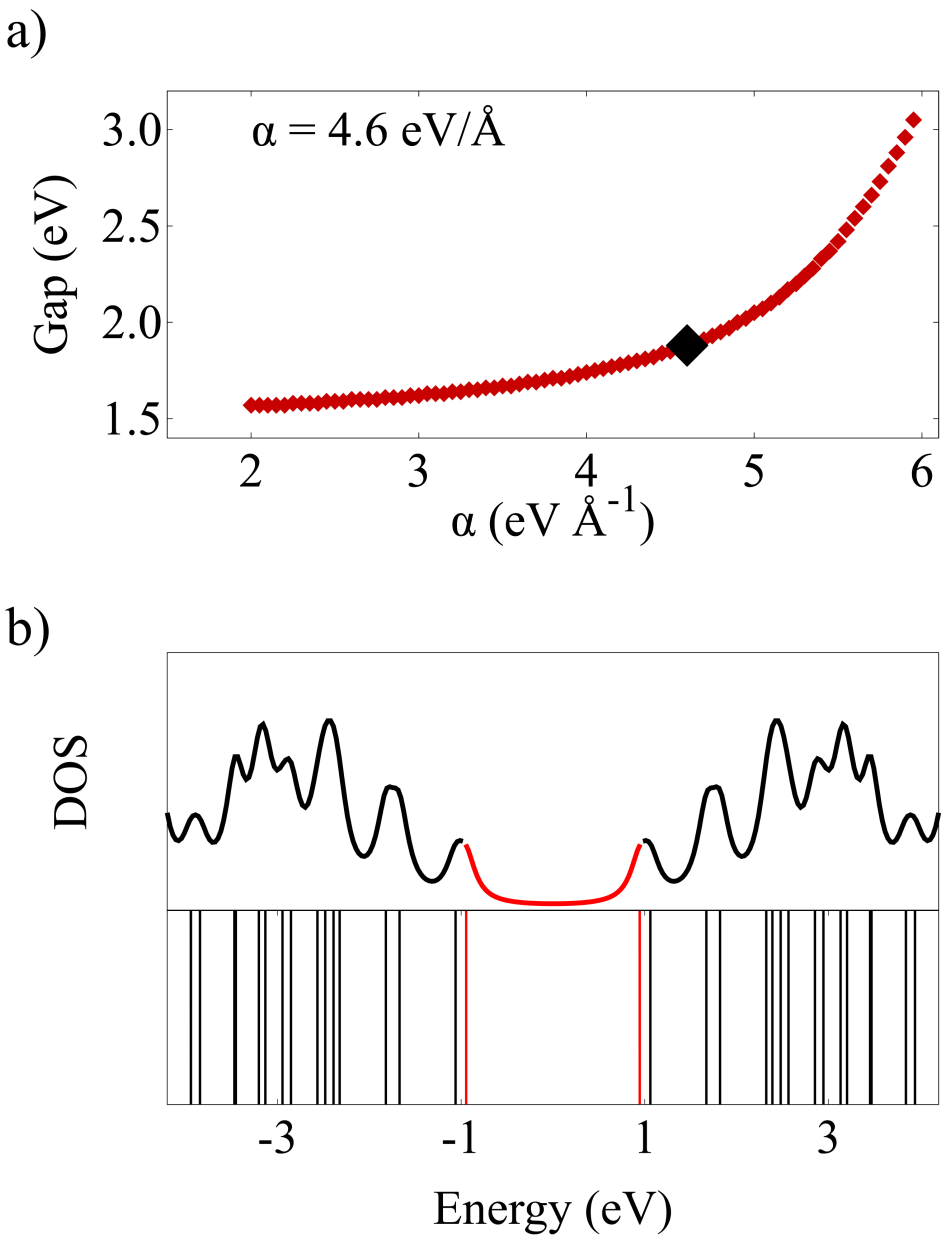

Figure 3.2: Electronic profile of the 4-CGNR. (a) shows the gap dependence over the electron-phonon coupling constant. As α increases, the gap rises accordingly. This happens since strong couplings make any electronic phenomena more energetically expensive. Therefore, the energy cost to promote a π-electron from HOMO to LUMO also grows. (b) displays the electronic band structure with the adequate α. In the upper side, this is shown via the density of the states. Below this graph, we display the respective energy levels.

which makes a non-zero gap emerge. In addition, the number of states around HOMO and LUMO increases. Similar behavior occurs in dimerized linear polymers and some AGNRs [63, 83, 74]. As for energies away from the forbidden region, the density grows notably higher, like in AGNRs. That said, preliminary analysis infers that 4-CGNR has similar electronic behavior to other GNRs.

3.2.2 λ gap tuning strategy

Once α is determined, we now proceed to investigate the previously discussed edge change. As stated before, zig-zag and armchair bonds are the building blocks of the cove-shaped edges. In that sense, we introduce a parameter that controls their proportion in the CGNR. Throughout this work, λ will refers to the distance between two adjacent armchair-like blocks. Increasing λ is the same as enforcing 4-CGNR to become more similar to ZGNRs. As a result, the nanoribbon preserves its cove-type edge, but some physical properties will change. Figures 3.3 and 3.4 show the gap response over two tuning strategies: λ variation and width changes. In figure 3.3, 2, 4, 6, and 8-CGNR responses are shown in orange, red, green, and blue, respectively. One can notice a common qualitative profile shared by all specimen when λ increases: a smooth monotonic gap decay that converges to 0 eV. That happens because rising λ makes CGNR resemble gradually more to zig-zag GNRs. Since ZGNRs present negligible energy bandgap, the resultant nanoribbon reproduce this trend.

Besides the similarities, each nanoribbon specimen experiences a unique decay rate. For instance, 2-CGNR exhibits gaps around 2.9-0.68 eV, while the 4-CGNR decay process begins in 1.88 and goes to about 0.04 eV. The other CGNRs share similar results. Such behavior

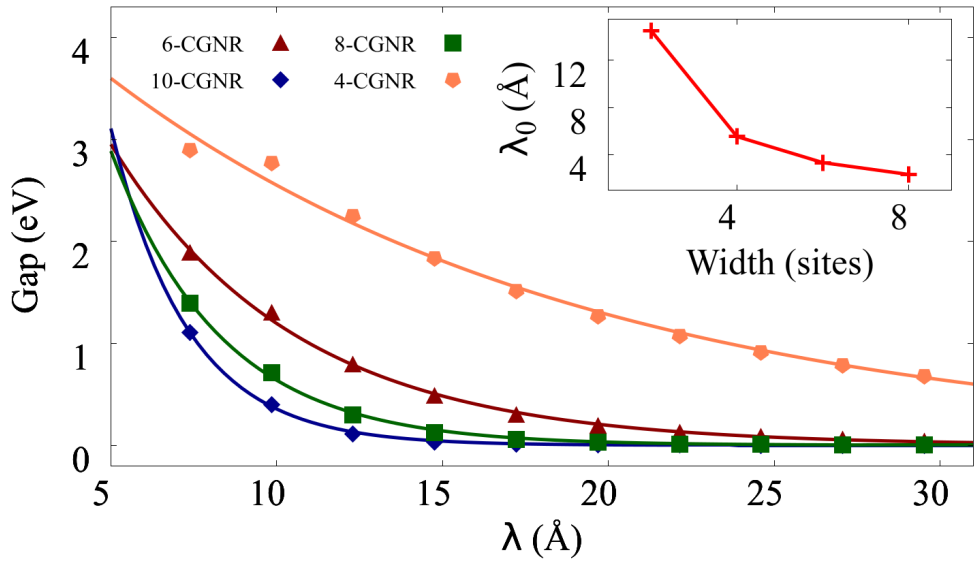

Figure 3.3: Gap response over λ variation. Each color/curve represents a CGNR specimen with a different width value. Orange, red, green and blue tones refers to 2-CGNR, 4-CGNR, 6-CGNR, and 8-CGNR, respectively. Regardless the nanoribbon width, all of them exhibit a smooth monotonic gap decay. Inset displays the characteristic length λ_0 fitted as a parameter of exponential function.

is due to quantum confinement effects. Among all specimen, 2-CGNR is the narrowest. Because of that, π-electrons will experience more intense quantum confinement. Hence, the gap rises. As a result, further λ increments will compete with more intense confinement, leading to a modest decay. Such behavior enforces smoother gap changes for narrower nanoribbons. This effect is better visualized by fitting the gap response (E_{gap}) in the following exponential decay function:

$$E_{gap} = E_0 \exp(-\lambda/\lambda_0), \tag{3.1}$$

in which E_0 is the gap for the lowest λ and λ_0 is a characteristic length that measures the decay intensity. The bigger λ_0 is, smoother the gap will drop. The inset of figure 3.3 shows the fitted parameter values for each CGNR width. As the width grows, λ_0 decreases. Therefore, narrower nanoribbons might present more abrupt gap variations. Moreover, results suggest that CGNR's

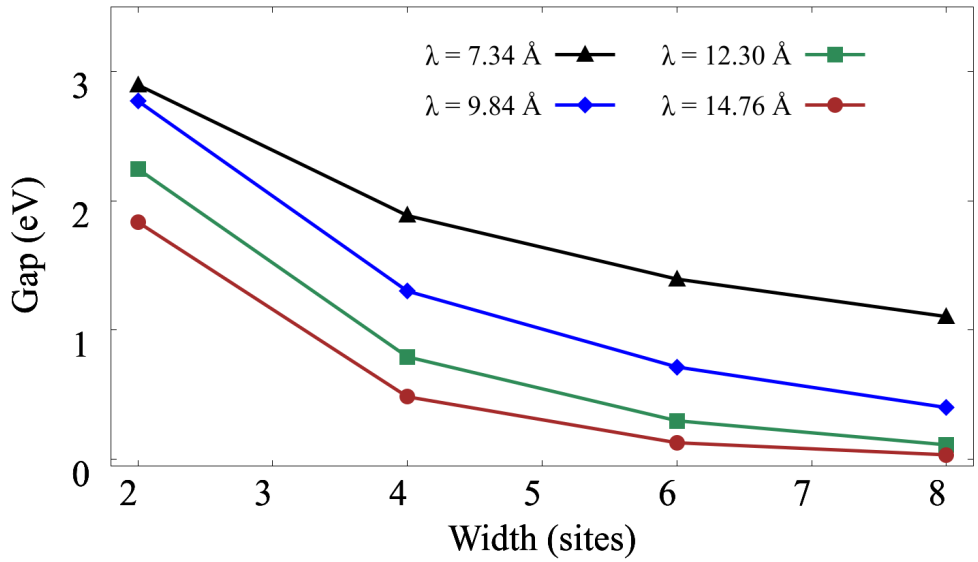

Figure 3.4: Influence of width changes in the electronic bandgap of cove-type GNRs. Each color indicates a different λ value. In all geometries, gap decays monotonically. Although width changes lead to similar outcomes, its decaying process is lesser smooth than λ tuning.

width restricts the tuning smoothness.

Figure 3.4 shows the results of another tuning strategy: width change for a given λ. Four λ cases are displayed, 7.34 Å, 9.84 Å, 12.30 Å and 14.76 Å. All curves present a monotonic gap decay as width increases. This behavior is a consequence of the weakening of quantum confinement effects. The wider a nanoribbon is, the narrower will be the energy shift between valence and conductance bands, translating into a decreasing bandgap. However, controlling the width leads to way less fluid gap transitions. For example, the $\lambda = 7.34$ Å case goes from 3 eV to almost 1 eV in only four steps, while 2-CGNR shows similar decay by transitioning through 10 steps. Therefore, the conventional width tuning strategy is not as smooth as the proposed λ procedure.

Throughout this work, ZGNRs present no bandgap due to the absence of spin-polarized

effects in our model [84, 85, 86]. The inclusion of such phenomena can induce gap opening [84, 85, 87, 26], although we expect no substantial changes in the results. In that scenario, given sufficient λ, each CGNR should converge to its correspondent ZGNR gap value. Regardless, the profile of each nanoribbon will remain the same: a smooth monotonic gap decay.

The presented results show accordance with previous works. Until now, most of the efforts aimed at the CGNR geometries with $\lambda = 7.38$Å [56, 35]. DFT-based investigations reports 6-CGNR and 8-CGNR with a gap of 1.508 [88] and 1.24 ∓ 0.03 eV [44], respectively. On the other hand, our method gives a gap of 1.394 eV for the former and 1.104 eV for the latter. Such tight agreement is expected since similar approaches for other GNRs produce comparable accuracy. For instance, simulations via local-density approximation (LDA) for the 5, 6, and 7-AGNRs estimate their gaps in 0.5, 1.1, and 1.65 eV, respectively [28, 26]. The same geometries present gaps of 0.55, 1.75, and 1.78 eV when our methodology is applied. This steady accordance trend, despite the nanoribbon type, reinforces the adequacy of our investigation approach.

3.2.3 The effects of gap tuning on the lattice

Although the effects of λ tuning on electronic properties are now clear, its influence on the lattice remains unknown. Figure 3.5 presents the 4-CGNR spatial profile as λ grows. In the left side, heat maps of bond length distortion for λ = 7.38 Å (a), 9.84 Å (b), 12.3 Å (c) and 14.76 Å (d) are displayed. Hot colors represent stretched bonds, while cold tones illustrate shrieked lengths. We measure the bond bend degree with respect to the equilibrium inter-site distance in graphene (1.41 Å). The respective bond length distribution of each nanoribbon is on

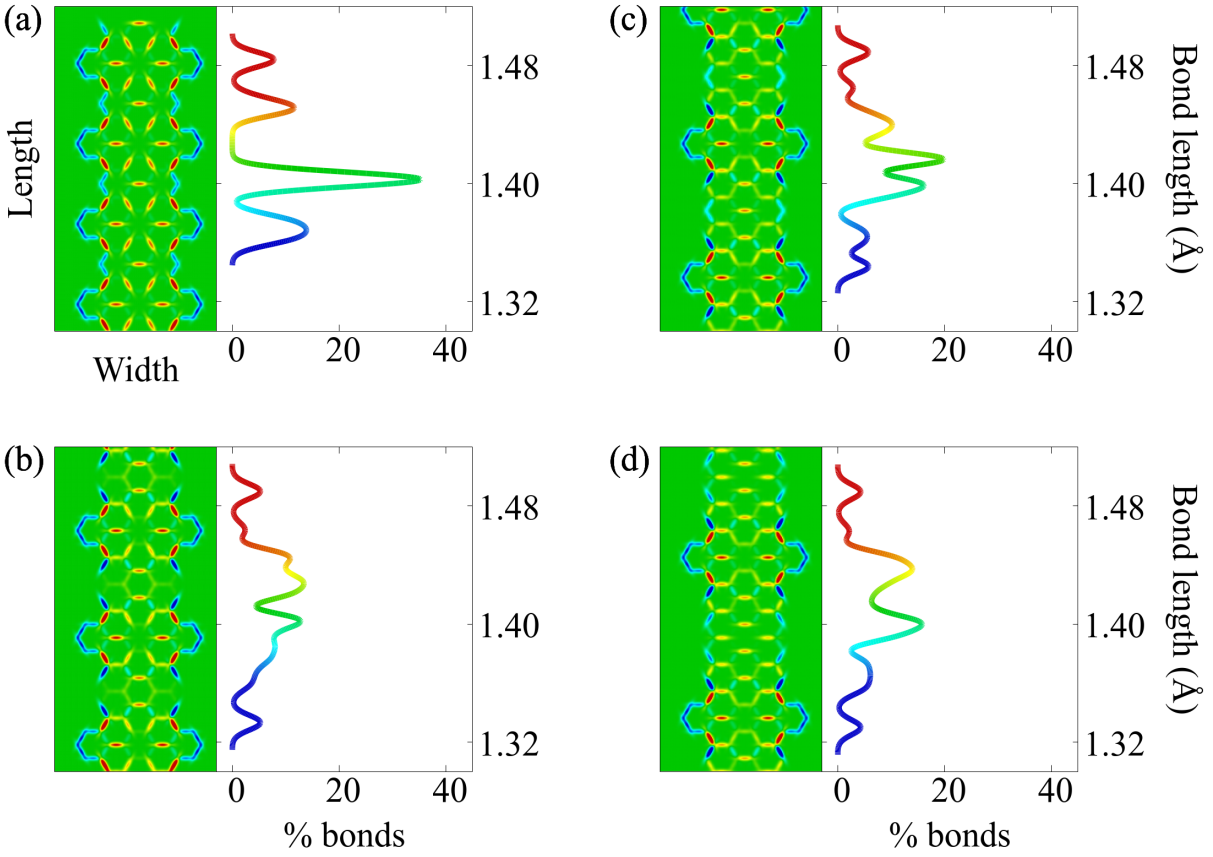

Figure 3.5: Collection of bond length heatmaps and their respective histograms for 4-CGNR geometries with (a) $\lambda = 7.38$ Å, (b) 9.84 Å, (c) 12.3 Å, and (d) 14.76 Å. Hot and cold colors indicate stretching and compression of bonds with respect to symmetric bond length, respectively. The histograms reveal that increases in λ induces changes in conjugation degree and increases the morphological spreading

the right side. Nonetheless, the distortion's magnitude is significantly smaller than the lattice parameter, regardless of the λ value. In all cases, deformities not greater than 4×10^{-2} Å occur. This magnitude represents less than 3 % of the equilibrium separation distance, which corroborates previous works [73, 89]. Moreover, these results reinforce the suitability of the harmonic approximations.

The bond pattern of the original 4-CGNR (λ = 7.38 Å) consists of two arrangements: a contraction-expansion alternation in the edges and a flower-like structure in the nanoribbon's core. In the edges, the proportion of contracted-type bonds outnumbers expanded-type ones.

Conversely, the core contains a significant amount of undistorted and stretched bonds. In this region, the aromatic rings surround every flower aggregate. The contribution of these two parts results in the histogram located on the right side. One can notice four prominent peaks: a green one located around the equilibrium bond length, a blue one centering in about 1.36 Å and two red-like ones in 1.45 and 1.485 Å. The green peak is the greatest of all four and represents almost 40 % of the lattice. The significant presence of undistorted bonds is due mostly to the aromatic rings in the core. Contrastingly, the blue peak results solely from the contracted bonds in the edges. As for the two hot-colored peaks, their origins differ. The more distorted one emerges from the expanded-type edges bonds, while the other rises from the flower structure.

As λ grows, the distortion profile changes accordingly. Notable differences already appear in the next configuration $\lambda = 9.84$ Å. The edge bonds still have an alternation pattern. However, undistorted bonds also appear between two adjacent armchair-like structures. Moreover, the flower-shaped pattern in the core disappears. Now, in this region, most of the edges become slightly stretched or contracted. As a result, these bonds move away from the aromatic length. Comparison with the corresponding histogram and the previous one reinforces this observation. The four prominent peaks are converted into seven timid crests. This dispersion increase changes the conjugation degree. Therefore, results suggest that injecting zig-zag chains in cove-type edges modifies lattice's conjugation.

As the final discussion, we are going to address the effects of width changes in cove-shaped GNRs. Figure 3.6 displays lattice distortion heatmaps for the 2-CGNR (a), 4-CGNR (b), 6-CGNR (c), 8-CGNR (d) for $\lambda = 7.38$Å. In the same fashion of Figure 3.5, hot and cold colors represent bond stretching and contraction, respectively. Moreover, each respective bond

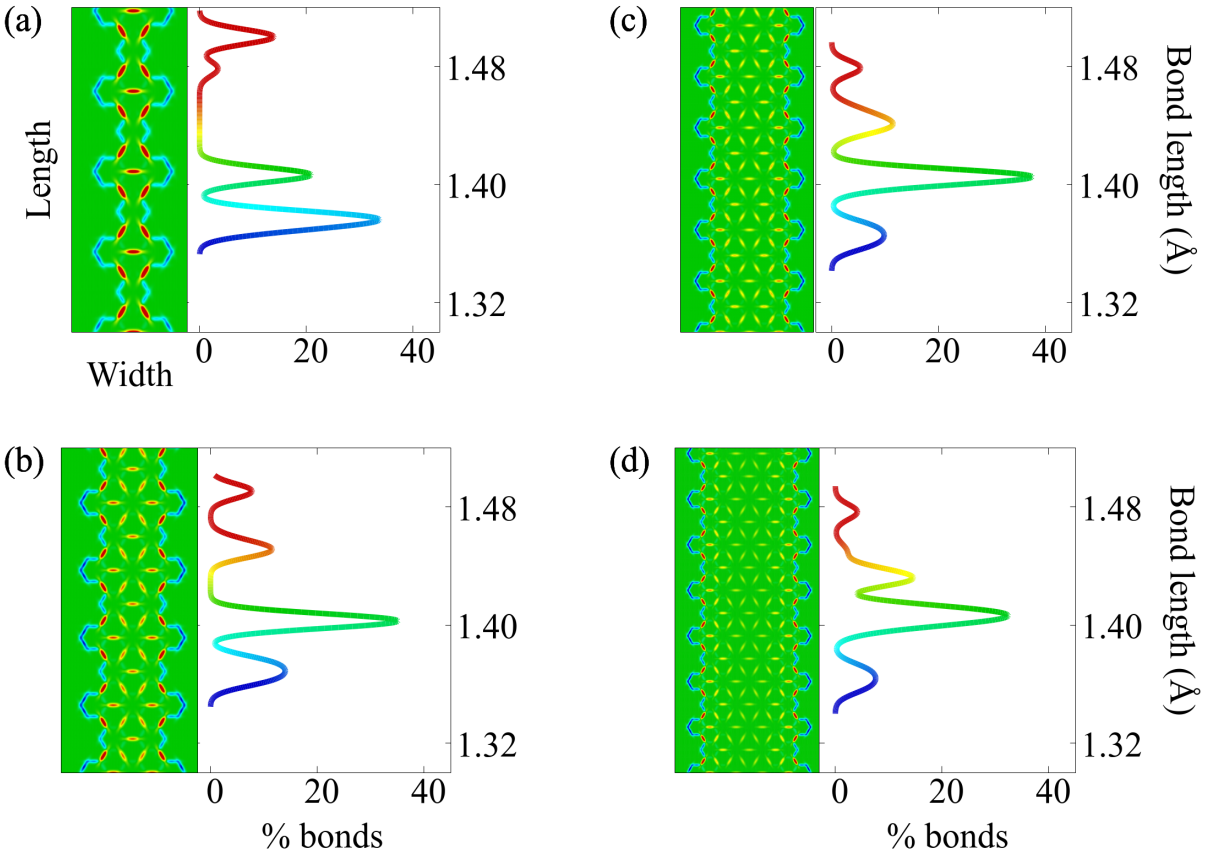

Figure 3.6: Lattice effects due to width changes in the CGNR. Sub-figures a, b, c, and d display the bond heatmap of 2, 4, 6, and 8-CGNR. The associated bond length distribution of each heatmap locates on its right side.

length distribution locates on the nanoribbon's right side. To some extent, all heatmaps present a similar appearance. In (a), edge bonds coordinate themselves in an alternation of contraction and stretching. Such pattern repeats in all simulated specimen. As for the core, we observe an interchanging pattern of green and red colored bonds. The associated distribution shows the lattice degree of distortion. One can see four peaks: a prominent one in the blue region, a minor crest centered close to 1.41 Å and two timid red peaks away from the aromatic length zone. The bonds in the edges contribute to the blue and the rightmost red peaks. Accordingly, the green and the leftmost red peaks account for the core bonds. We placed black dashed guidelines centering on each peak in (a) to aid association with the other distributions.

Figures 3.6(b)-(d) shows the effects of increasing the width in cove-type GNRs. In 3.6(b), the 4-CGNR lattice profile is displayed. As discussed previously, this specimen has a characteristic bond profile in the edges and the core. The former consists of an alternation of deformed bonds like in the 2-CGNR. However, the increase in the width entirely changes the bonds located in the core region. Now, a distinctive flower-like structure appears along with aromatic rings. The rising of these core bonds dramatically changes the bond distribution. There are still four peaks, but their position and intensities are different. In this case, we have a prominent green, a blue one close to the aromatic length, and two red crests. As one can observe, the proportion of green and light-red bonds grows at the expense of blue ones. That happens due to the contribution of the core bonds. The existence of the flower structure and the adjacent green bonds shifts the balance of the bond population.

Further width increases will intensify this trend. As can be seen in 3.6(c) and 3.6d), enlarging the nanoribbon causes two substantial changes: an increase of core bonds and a weak-

ening of the deformations in the flower structure. As a result, lightly stretched and undistorted bonds contribute more to the distribution. Then, the bond distribution tends to concentrate around the green region. This trend remains until the width becomes so large that the edge bonds contribution turns negligible. At that stage, CGNRs exhibit a profile similar to pure zig-zag GNRs. In addition, λ tuning seems to provoke a more deep morphological alteration in the CGNRs.

3.3 Conclusion

In this work, we studied a potential edge change strategy that allows gap tuning in the CGNR. The simulations were carried via the SSH model that accounts for the coupling between lattice and electronic phenomena. Before digging into the problem, we first determined the suitable electron-phonon coupling constant (α) for the CGNR to be 4.6 eV/Å. Comparison with later reports confirms that CGNRs and AGNRs have a similar lattice-electronic response.

Next, we proceeded to carry the edge change modifications. Results show that increasing the proportion of zig-zag edges in CGNR leads to a smooth gap drop. This conclusion becomes even more evident when compared with width-change strategies. Therefore, due to the unique shape of the CGNRs, they can endure a gap-tuning procedure more efficiently than standard tuning approaches, showing smooth access to 40 gap values lying within the range of 0-3 eV. This feature contributes to the potential of such GNRs since it allows deeper tailoring of the physical properties.

In addition, we also investigated the changes in the lattice as the tuning procedure

unravels. We found that increasing the proportion of zig-zag edges leads to a systematic morphological spreading in the bond length distribution. On the other hand, changes in the width of the CGNR provoke distinct effects. As the width increases, the bond length distribution becomes more concentrated around the aromatic bond length. Thus, both strategies are physically different.

The results obtained indicate that carrying such structural changes in the CGNR may produce new materials with interesting electronic properties. As possible extension to this work, we intend to explore the charge transport in the transformed morphology through dynamical simulations of charged states. By doing that, we hope to characterize the charged quasiparticles and their role in the transport, as well as the effects of structural changes in the phenomena.

CHAPTER 4

PUBLISHED ARTICLE (RSC ADVANCES)

RSC Advances

PAPER

View Article Online
View Journal | View Issue

Cite this: *RSC Adv.*, 2020, **10**, 26937

Smooth gap tuning strategy for cove-type graphene nanoribbons

Tiago de Sousa Araújo Cassiano, [a] Fábio Ferreira Monteiro, [a] Leonardo Evaristo de Sousa,[b] Geraldo Magela e Silva[a] and Pedro Henrique de Oliveira Neto *[a]

Received 2nd April 2020
Accepted 29th June 2020

DOI: 10.1039/d0ra02997a

rsc.li/rsc-advances

Graphene is a carbon-based material with an extensive range of promising properties. Since it does not present a bandgap, graphene is not suitable for optoelectronic applications. One possible way to open a gap is achieved by reducing graphene to its nanoribbon (GNR) form. Recently, a GNR with well defined cove-type periphery proper for large-scale production was synthesized showing an energy bandgap of 1.88 eV. In this work, we propose an edge termination strategy that allows for smoothly tuning the energy bandgap of cove-type GNRs by systematically changing the periodicity with which armchair-like and zigzag-like edges alternate. Using an extended two-dimensional Su–Schrieffer–Heeger tight-binding model we compare the effects of this edge termination process on lattice deformation with those arising from changes in nanoribbon width. Results show that modifications to the edges of cove-type GNRs are able to smoothly reduce energy bandgaps at the expense of losses in conjugation and increased morphological spreading. Energy band gap values starting from ≈3 eV to almost 0 eV were obtained. The flexibility provided by this gap tuning procedure places the cove-type GNR as an interesting candidate material for optoelectronic applications.

I. Introduction

Graphene is a two-dimensional system composed of honeycomb lattices of carbon atoms. It hosts a broad set of interesting physical properties,[1–5] resulting in the development of many graphene based applications.[6–9] A drawback prevents the use of these materials in optoelectronic devices: the absence of an energy bandgap, which is the hallmark of semiconductor materials. However, bandgap opening can be achieved by means of several approaches, such as a doping procedures,[10–12] which consist in the addition of non-carbon atoms into the lattice. The injection of these atoms induces a symmetry break in the system, leading to the appearance of a gap. Another way to engineer a gap opening is through the reduction in one of the dimensions of the graphene sheet until it reaches atomic scales (several angstroms). These quasi one-dimensional graphene strips are known as graphene nanorribons (GNRs).[13,14] Due to their limited size, quantum confinement effects may arise, resulting in larger bandgaps. It is expected that GNRs will begin the next generation of semiconductor applications.[15–17]

The properties of GNRs are directly related to their geometries, with edge structure and width extension playing a key role on the electronic properties.[18] Two edge shapes, known as zigzag (ZGNR) and armchair (AGNR) are specially relevant. These AGNRs are usually classified by the number N_a of atoms along their width (N_a-AGNR) and may be divided in three families. These families are defined by $N_a = 3p + 2$, $3p + 1$ and $3p$, where p is a positive integer. Importantly, ZGNRs and AGNRs from the $3p + 2$ family do not present appreciable bandgaps, but, on the other hand, AGNRs from $3p$ and $3p + 1$ show semiconductor properties.[13]

Recently, a graphene nanoribbon with a new edge termination was synthesized using a bottom-up liquid-phase procedure.[19] The resultant GNR presented a cove-shaped edge (Fig. 1), which may be seen as a combination of the armchair and zigzag borders. Fig. 1(a) highlights examples of both border types inside the CGNR, with a sample of an armchair and zigzag border highlighted in red and blue, respectively. The synthesis technique employed relies on the use of smaller compounds through chemical reactions allowing an atomically precise design that mitigates structural defects and controls the proportion of each edge type. Known as cove-type GNR, or CGNR, this new nanoribbon architecture was reported as structurally well-defined and unusually long (>200 nm).[19]

Gap tuning can be performed by modifying the AGNR's width.[13,20,21] However, since each AGNR family presents a particular gap dependence, this tuning procedure becomes complex. For instance, the difference between the energy bandgap of a 3-AGNR and 4-AGNR is about 0.18 eV.[13] On the other hand, the gap variation between 4-AGNR and 5-AGNR is approximately 2 eV. As such, a smooth gap tuning procedure based on width changes in AGNRs is not possible.

[a]*Institute of Physics, University of Brasília, Brazil. E-mail: pedrohenrique@unb.br*
[b]*Theoretical and Structural Chemistry Group, State University of Goias, Anapolis, Goias, Brazil*

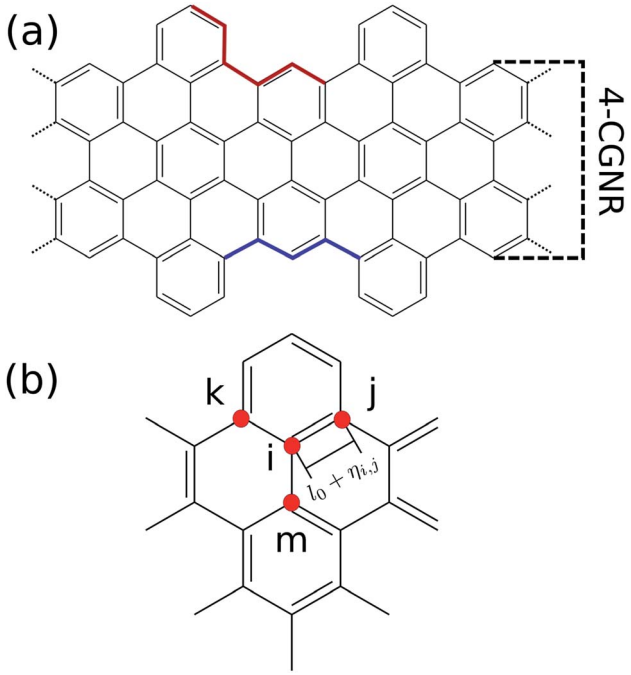

Fig. 1 (a) Chemical structure of a 4 atoms wide cove-type GNR. The armchair-like and zigzag-like edges are highlighted in red and blue, respectively. (b) Site indexation used in the two-dimensional SSH model.

Another possible strategy to tune energy gap relies on edge changes. The literature provides several successful attempts based on morphological transformation.[22–25] Nanopores placed on GNR's lattice are an example.[26] The defect produced by the hole induces the formation of V-shaped edges. This new border is a hybridization of armchair-like and zig-zag structures and controlling their relative amounts enables a smooth tuning procedure to be undertaken. As mentioned before, CGNRs can have its edge modified by a similar strategy. The question then arises as to how such changes may affect the electronic properties of these nanoribbons, as this could constitute a reliable method for gap tuning in GNRs.

To address the aforementioned issue, in this work, we simulated several cove-edge terminations to investigate both energy bandgap and conjugation changes in CGNRs. The nanoribbons were modelled using a two dimensional Su–Schrieffer–Heeger (SSH) model Hamiltonian. By means of a self consistent field approach, we evaluated the bond length distribution taking into consideration both electronic and phonon degrees of freedom. Our results show that changes in a single parameter that characterizes edge terminations leads to a monotonically decrease in the energy bandgap. By relating the bond length distribution pattern with the energy gap, this phenomenon is shown to be a consequence of the superposition of armchair and zigzag architectures. Gap values ranging from ≈3 eV to almost 0 eV were reached, showing that this method may be suitable for tailoring GNRs for very specific applications.

II. Methods

The methodology applied in this work is similar to the methodology used in previous works of our group.[27–30] The GNRs are simulated through the two dimensional extended SSH model, which starts with a Hamiltonian $H = H_{\text{latt}} + H_{\text{tb}}$, where H_{latt} refers to the lattice Hamiltonian and H_{tb} corresponds to the electronic part. The lattice term reads

$$H_{\text{latt}} = \frac{K}{2}\sum_{\langle i,j\rangle}\eta_{i,j}{}^2 + \frac{1}{2M}\sum_i P_i^2, \tag{1}$$

where i and j index neighboring sites, K is the harmonic oscillator constant, P_i is the momentum of i-th site, M is the site's mass and $\eta_{i,j}$ is the relative displacement between the i and j neighboring sites (Fig. 1(b)). This means that, for instance, the distance between the site i and site j is $l_0 + \eta_{i,j}$, in which l_0 is the bond length of a fully symmetric lattice (1.41 Å). The $\langle i,j \rangle$ term within the summation indicates a pair-wise sum.

As can be seen, the lattice part of the Hamiltonian corresponds to classical harmonic approximation. This is adequate since typical bond length variations in GNRs are usually not greater than 2%.[29] On the other hand, the electronic terms are treated quantum mechanically by means of the second quantization formalism, modelling the π-electrons in a tight-binding approach. This electronic Hamiltonian is given by

$$H_{\text{tb}} = -\sum_{\langle i,j,s\rangle}\left[\left(t_0 - \alpha\eta_{i,j}\right)C_{i,s}^{\dagger}C_{j,s} + h.c\right], \tag{2}$$

where the operator $C_{i,s}^{\dagger}$ is the creation operator of π-electron in i-th site with spin s. $C_{i,s}$ is the corresponding annihilation operator. The lattice and electronic parts of the model are connected by the inclusion of an electron–phonon coupling (α) in the tight-binding's hopping term, in which t_0 is the hopping integral for a symmetric lattice. The coupling between the electronic and lattice parts allows a more accurate description of these materials.

The description of our system is based on the set $\{\eta_{i,j}\}$ and the eigenvectors of H, $\{\psi_k(i)\}$. However, these very set are required to evaluate the equations of motion. The problem can be solved by employing a self-consistent approach. An initial guess of $\{\eta_{i,j}\}$ (usually $\{\eta_{i,j}\} = 0$) is chosen. Then, the Hamiltonian can be numerically calculated. With this procedure, the Schrödinger equation turns into an eigenvalue problem. The diagonalization process yields the eigenvectors $\{\psi_k(i)\}$. The expected value of Lagrangian, $\langle L\rangle = \langle\Psi|L|\Psi\rangle$, where $|\Psi\rangle$ is the Slater determinant is used in the Euler–Lagrange equation,

$$\frac{\mathrm{d}}{\mathrm{d}t}\left(\frac{\partial\langle L\rangle}{\partial\dot{\eta}_{i,j}}\right) = \frac{\partial\langle L\rangle}{\partial\eta_{i,j}}. \tag{3}$$

The solutions of these equations yield a new set of $\{\eta_{i,j}\}$. The process is repeated. Once the iteration converges, the final set of $\{\eta_{i,j}\}$, along with the associated eigenvectors and eigenvalues give the stationary state of the CGNR.

The Hamiltonian's parameters were chosen in accordance with previous works, for which $t_0 = 2.7$ eV (ref. 31) and $K = 21$ eV

Å^{-2}.[32] As for the electron–phonon constant, its evaluation is done through a semi-empirical procedure which will be described in the results session. Finally, as the number of carbon atoms on the width classifies armchair graphene nanoribbons, the same criterion will be applied throughout this work. For instance, the CGNR from Fig. 1(a) exhibits four carbons along the width axis, therefore, we refer to it as 4-CGNR. For the length direction, periodic boundary conditions are employed.

III. Results

As mentioned before, the electron–phonon constant α connects the dynamics of the π electrons with that of the lattice, affecting the energy bandgap. However, α cannot be easily measured directly,[28] thus requiring an indirect method for its evaluation. Since the energy bandgap can be effectively determined experimentally, the appropriate electron–phonon constant is then determined to be the one that reproduces the experimental measure. For the cove-type 4-CGNR illustrated in Fig. 1(a), the optical bandgap is reported to be 1.88 eV.[19] The gap is determined by the energy difference of eigenvalues of CGNR in a neutral state, which amounts to the optical gap. The formation of excitons is not considered as no relaxation process takes place. Fig. 2(a) shows the dependence between α and the energy bandgap, from which a coupling of 4.6 eV Å^{-1} is found to best reproduce the experimental results. AGNRs, for instance, present acceptable couplings values that range from 3.5 to 5.5 eV Å^{-1}.[33] Since the CGNR's α lies within this interval, the coupling between the lattice and electrons is observed to be roughly the same as in AGNRs.

The nanoribbon represented in Fig. 1(a) has its energy levels shown in Fig. 2(b). Where the valence and conduction bands consists of all lines below and above 0 eV, respectively. The highest occupied molecular orbital (HOMO) and the lowest unoccupied molecular orbital (LUMO) are highlighted in red, from which the 1.88 eV bandgap is obtained. It can be seen that some regions in the spectrum present an accumulation of energy levels in close proximity. This is better visualized by calculating the density of states as a function of energy (DOS). The DOS of the 4-CGNR of Fig. 1(a) is displayed on the right side of Fig. 2(b). Within the gap region, the DOS is identically zero. This forbidden zone arises as a result of the symmetry break induced by the edge termination of the cove-type GNR. The same effect occurs, for example, in polyacetylene, where the gap opens when a dimerized configuration is enforced. Furthermore, the appearance of an energy gap changes the profile of allowed states as well, with an increase in the number of energy levels near the HOMO and LUMO. This translates into the appearance of a peak close to those states, as seen in Fig. 2(b). Additionally the DOS tends to present high values even for energies away from the gap region. This behavior is shared with semiconductor AGNRs.[34]

Once the electron–phonon coupling has been determined, we may explore possible means of edge termination in CGNRs. As we have seen, the cove shaped edges are formed by alternating armchair and zigzag bond types. The periodicity of such

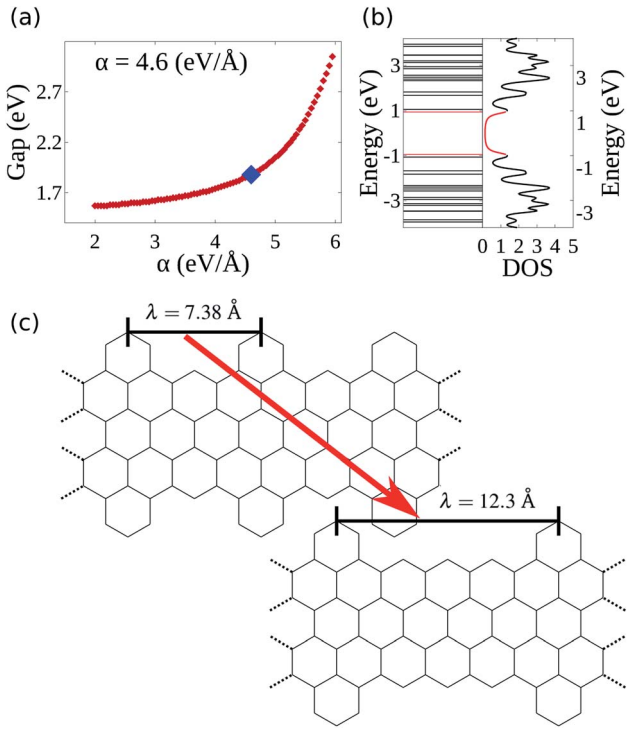

Fig. 2 (a) Energy bandgap of the 4-CGNR of Fig. 1(a) as a function of the electron–phonon coupling constant (α). The coupling that coincides with the experimentally measured energy bandgap is the one which best represents the CGNRs. (b) Energy levels and corresponding density of states of a 4-CGNR with $\alpha = 4.6$ eV Å^{-1}. (c) Example of the edge termination process. λ indicates the periodicity of the alternation between armchair and zigzag-like edges.

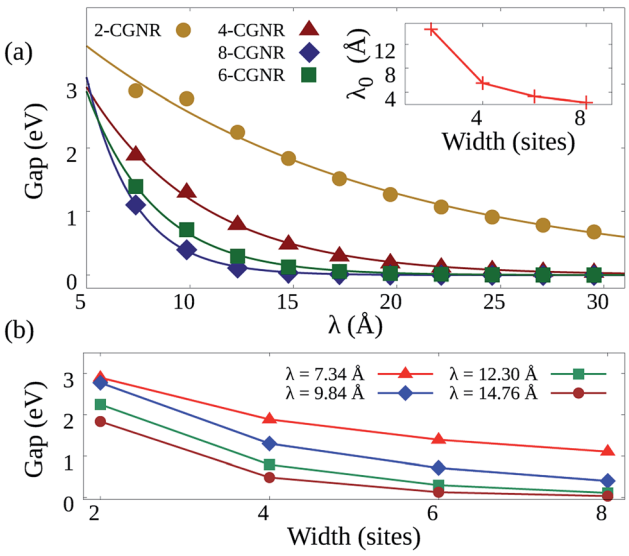

Fig. 3 (a) Bandgaps as a function of λ for CGNRs of several widths. Each symbol represents a width and the lines are fits to the data considering an exponential decay. The inset highlights the behavior of the decay constant for each width. (b) Bandgap dependence on width for fixed λ values. Lines are guides for the eye.

alternation is measured by the parameter λ, which corresponds to the distance between two neighboring armchair-like edges (Fig. 2(c)). An increase in λ is equivalent to an increase in the proportion of zigzag to armchair edges. This zigzag bond injection procedure maintains the GNR with a cove-type periphery, but modifies its properties. Fig. 3(a) exhibits the effect of zigzag bond injection on the energy bandgap of CGNRs of different widths as a function of the parameter λ. As λ increases, the gap decays monotonically for all widths. This stems from the fact that as λ increases, the resultant nanoribbon resembles progressively more a pure zigzag GNR, which is known to present no energy bandgap. As such, the modification of the parameter λ in cove-type GNRs allows for a smooth and almost continuous gap tuning procedure.

The general decay profile of bandgaps with λ is shared by all widths. However, the decay rates are different for each CGNR, which results in different ranges of allowed gaps. For instance, 2-CGNR presents gaps ranging from about 0.68 eV to 2.90 eV. On the other hand, 4-CGNR starts at 1.88 eV and decays until nearly 0.04 eV. A steeper decay trend is seen for the broader nanoribbons, with 8-CGNR showing bandgaps that range from 1.10 eV until 0.00 eV. All of them converge close to 0 eV given a sufficiently long zig-zag edge chain. Pure ZGNRs present almost no gap when spin-polarization effects are not taken into account.[35–37] Thus, the CGNR exhibits no significant additional contribution when it reaches the asymptotic region. This systematic decrease in gap magnitude is due to the reduction in quantum lateral confinement that takes place when nanoribbon width is increased.[38] This effect can be quantified by fitting the data in Fig. 3(a) with a function $E_{gap} = E_0 \exp(-\lambda/\lambda_0)$, where λ_0 is a characteristic length. This λ_0 parameter is shown in the inset of Fig. 3(a) and decreases with nanoribbon width. Larger values of λ_0 indicate the possibility of smoother tuning of the energy bandgap. As such, nanoribbon width may become a limiting factor for this tuning procedure.

Our model does not consider spin-polarized effects. This choice may have an direct influence on ZGNRs[13,35,36,39] since spin-polarized simulations report this nanoribbon to be a semiconductor with magnetic properties.[37] The width of each ZGNR inside the CGNR changes the gap value reached on the asymptotic regime, and it is reasonable to infer that the addition of spin-polarization will contribute to enlarger the final gap. Each CGNR converges to a specific gap value, depending on its width.

Density functional theory (DFT) studies regarding CGNRs are mostly concerned with geometries with $\lambda = 7.38$ Å.[40,41] The gap values found in these works are in agreement with our results. For instance, 6-CGNR calculates a gap of 1.508 eV (ref. 42) while our simulated tight-binding model presented a gap of 1.394 eV. 8-CGNR's bandgap is estimated as 1.24 ± 0.03 eV.[43] On the other

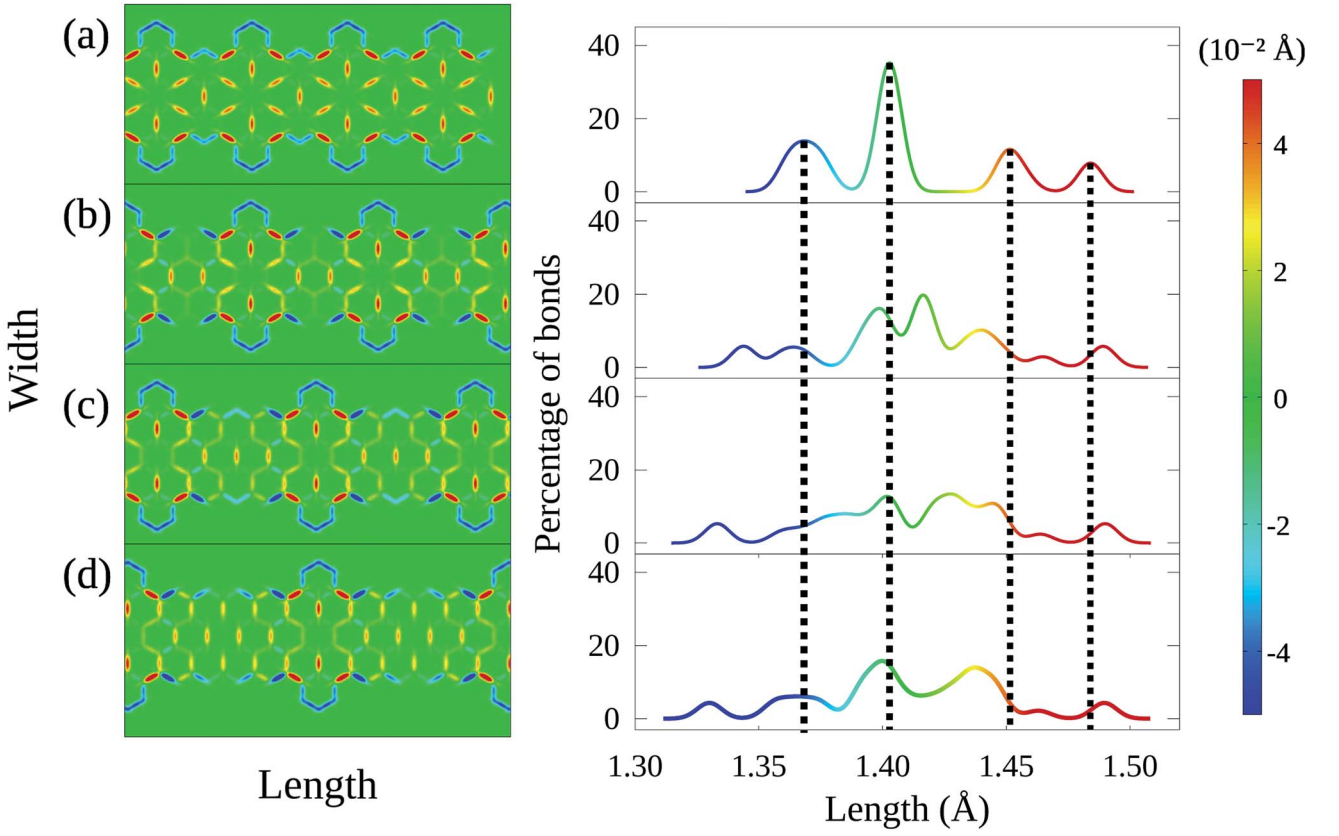

Fig. 4 Bond length distortion heatmap and their corresponding histograms for 4-CGNR geometries with (a) $\lambda = 7.38$ Å, (b) $\lambda = 9.84$ Å, (c) $\lambda = 12.3$ Å, and (d) $\lambda = 14.76$ Å. Hot and cold colors indicate stretching and compression of bond lengths with respect to 1.41 Å, respectively. The histograms indicate that increases in λ induces changes in conjugation and increased morphological spreading.

hand, our calculations showed a gap of 1.104 eV. This accordance trend is shared with AGNR as well. For instance, LDA calculations show 5, 6, and 7-AGNR with, respectively, $\approx$0.5, 1.1, 1.65 eV.[13,21] Our method evaluates the gap from the same geometries, respectively, 0.55, 1.75, 1.78 eV. This visible agreement shows the suitability of the presented methodology.

The effects of varying nanoribbon width for a given λ can be seen in Fig. 3(b). In wider nanoribbons, quantum confinement effects become weaker, reducing energy bandgaps accordingly. A similar dependence between gap and width size has been observed in AGNRs as well.[13] However, it is also clear that changes in width do not produce bandgap reductions as smooth as those observed by increasing λ. This is so because, by preserving the edge structure, changes in width do not translate into a transformation from armchair-like to zigzag-like nanoribbons, which possess completely different bandgap properties. As such, controlling nanoribbon width does not constitute a tuning procedure as effective as controlling λ.

Modifications in energy bandgap are associated with structural changes in graphene nanoribbons. In this sense, it is worth looking into how the edge termination described here affects the nanoribbon's morphology. Fig. 4 presents on the left heatmaps corresponding to bond length distortions for four 4-CGNRs of different λ (λ = 7.38, 9.84, 12.3 and 14.76 Å). Hot and cold colors indicate, respectively, stretching and contraction of bond lengths with respect to the 1.41 Å carbon–carbon bond length found in graphene. The magnitude of bond distortions reaches at most 0.04 Å, or roughly 3% of the original bond length, in agreement with similar works.[28,44] On the right of Fig. 4, histograms present the distribution of bond lengths in each CGNR.

Results for the original 4-CGNR (Fig. 4(a)) are characterized by four well defined peaks in the histogram, which are marked by vertical dashed lines for the sake of comparison with the other cases. As it can be seen, this histogram indicates that almost 40% of the bonds in this nanoribbon do not suffer significant distortion. These bonds correspond mostly to the aromatic rings that lie at the center of the flower-like pattern seen in the heatmap on the left. These flower-like structures result from the stretching of the bonds between the aromatic rings and the exterior carbons. On the other hand, the edge bonds are seen to contract strongly, corresponding to the leftmost peak observed in the histogram.

As λ increases, variation ensues. The well defined peak structure is seen to spread, with bond lengths being distributed more uniformly as λ grows larger (Fig. 4(b)–(d)). Although the behavior of edge bonds remains the same for all cases, the flower-like structures are no longer seen as the number of hexagonal rings diminishes. In fact, these structures are observed only in middle of regions whose edges are armchair-like. As such, we associate modifications in λ to changes in the conjugation of CGNRs.

Finally, we perform a similar analysis considering increases in nanoribbon width for a fixed λ. Fig. 5 confirms the aforementioned relationship between conjugated bonds and the presence of armchair-like edges, as the flower-like structures are

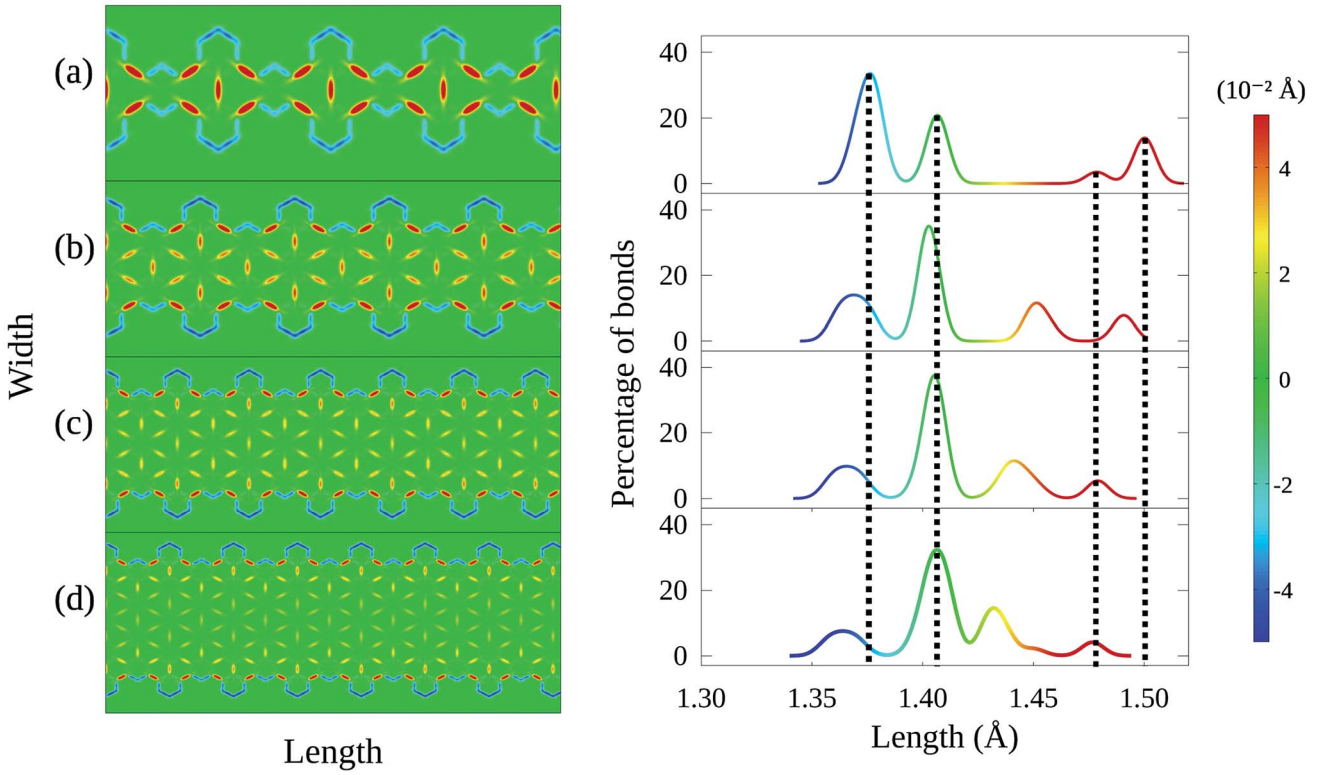

Fig. 5 Bond length distortion heatmap and their corresponding histograms for (a) 2-CGNR, (b) 4-CGNR, (c) 6-CGNR and (d) 8-CGNR. All CGNRs shown here have λ = 7.38 Å. The histograms show that conjugation is preserved with width changes.

seen in all cases but the first, for which border effects are dominant. In addition, the histograms indicate that width increases may shift the position of the peaks, but do not produce the morphological spreading observed in the cases of varying λ. These results demonstrate that the edge termination process produces much more profound changes in the CGNR's properties, beyond bandgap modulation.

IV. Conclusions

In conclusion, we have determined the electronic and morphological structures of cove-type GNRs by means of a two-dimensional extented SSH model. Comparing simulations with experimental results, it was possible to determine the electron–phonon coupling in this kind of nanoribbon to be 4.6 eV $Å^{-1}$. An edge termination procedure was investigated and it was determined to constitute a smooth and nearly continuous gap tuning scheme as long as nanoribbon width is kept sufficiently small. Furthermore, it was demonstrated that this termination procedure leads to increases in morphological spreading accompanied by reduction in the conjugation of the nanoribbons. Finally, it was determined that even though width modifications do not result in morphological disorder, they are not as effective a tool for gap tuning.

Throughout this work, no heterogeneous cases were held. Thus, the real effects of the studied edge change are unknown to us. However, considering the results obtained, we may expect no substantial changes. The entire geometry will lose its symmetry but, locally, every combination of armchair–zigzag–armchair structures will remain itself as a cove-shaped edge. The tuning procedure will remain available. As for the lattice distortion profile, we would expect changes on the histogram peaks.

Conflicts of interest

There are no conflicts to declare.

Acknowledgements

The authors gratefully acknowledge the financial support from Brazilian Research Councils CNPq, CAPES, and FAPDF. P. H. O. N, and G. M. S. gratefully acknowledge, respectively, the financial support from FAP-DF grants 0193.001662/2017, and 0193.001766/2017. G. M. S. gratefully acknowledge the financial support from CNPq grants 304637/2018-1.

References

1 A. C. Neto, F. Guinea, N. M. Peres, K. S. Novoselov and A. K. Geim, The electronic properties of graphene, *Rev. Mod. Phys.*, 2009, **81**, 109.
2 A. A. Balandin, S. Ghosh, W. Bao, I. Calizo, D. Teweldebrhan, F. Miao and C. N. Lau, Superior thermal conductivity of single-layer graphene, *Nano Lett.*, 2008, **8**, 902.
3 A. Rozhkov, A. Sboychakov, A. Rakhmanov and F. Nori, Electronic properties of graphene-based bilayer systems, *Phys. Rep.*, 2016, **648**, 1.
4 C. Song, X. Yin, M. Han, X. Li, Z. Hou, L. Zhang and L. Cheng, Three-dimensional reduced graphene oxide foam modified with zno nanowires for enhanced microwave absorption properties, *Carbon*, 2017, **116**, 50.
5 Z. Lei, J. Zhang, L. L. Zhang, N. A. Kumar and X. Zhao, Functionalization of chemically derived graphene for improving its electrocapacitive energy storage properties, *Energy Environ. Sci.*, 2016, **9**, 1891.
6 W. Choi, I. Lahiri, R. Seelaboyina and Y. S. Kang, Synthesis of graphene and its applications: a review, *Crit. Rev. Solid State Mater. Sci.*, 2010, **35**, 52.
7 Z. Sun, A. Martinez and F. Wang, Optical modulators with 2d layered materials, *Nat. Photonics*, 2016, **10**, 227.
8 F. Koppens, T. Mueller, P. Avouris, A. Ferrari, M. Vitiello and M. Polini, Photodetectors based on graphene, other two-dimensional materials and hybrid systems, *Nat. Nanotechnol.*, 2014, **9**, 780.
9 A. L. M. Reddy, A. Srivastava, S. R. Gowda, H. Gullapalli, M. Dubey and P. M. Ajayan, Synthesis of nitrogen-doped graphene films for lithium battery application, *ACS Nano*, 2010, **4**, 6337.
10 H. Liu, Y. Liu and D. Zhu, Chemical doping of graphene, *J. Mater. Chem.*, 2011, **21**, 3335.
11 J. Dai and J. Yuan, Adsorption of molecular oxygen on doped graphene: atomic, electronic, and magnetic properties, *Phys. Rev. B: Condens. Matter Mater. Phys.*, 2010, **81**, 165414.
12 P. Rani and V. Jindal, Designing band gap of graphene by b and n dopant atoms, *RSC Adv.*, 2013, **3**, 802.
13 Y.-W. Son, M. L. Cohen and S. G. Louie, Energy gaps in graphene nanoribbons, *Phys. Rev. Lett.*, 2006, **97**, 216803.
14 X. Li, X. Wang, L. Zhang, S. Lee and H. Dai, Chemically derived, ultrasmooth graphene nanoribbon semiconductors, *Science*, 2008, **319**, 1229.
15 L. Jiao, L. Zhang, L. Ding, J. Liu and H. Dai, Aligned graphene nanoribbons and crossbars from unzipped carbon nanotubes, *Nano Res.*, 2010, **3**, 387.
16 H. Chang and H. Wu, Graphene-based nanomaterials: synthesis, properties, and optical and optoelectronic applications, *Adv. Funct. Mater.*, 2013, **23**, 1984.
17 D. Prezzi, D. Varsano, A. Ruini, A. Marini and E. Molinari, Optical properties of graphene nanoribbons: the role of many-body effects, *Phys. Rev. B: Condens. Matter Mater. Phys.*, 2008, **77**, 041404.
18 M. Ezawa, Peculiar width dependence of the electronic properties of carbon nanoribbons, *Phys. Rev. B: Condens. Matter Mater. Phys.*, 2006, **73**, 045432.
19 A. Narita, X. Feng, Y. Hernandez, S. A. Jensen, M. Bonn, H. Yang, I. A. Verzhbitskiy, C. Casiraghi, M. R. Hansen, A. H. Koch, *et al.*, Synthesis of structurally well-defined and liquid-phase-processable graphene nanoribbons, *Nat. Chem.*, 2014, **6**, 126.
20 M. Y. Han, B. Özyilmaz, Y. Zhang and P. Kim, Energy band-gap engineering of graphene nanoribbons, *Phys. Rev. Lett.*, 2007, **98**, 206805.

21 L. Yang, C.-H. Park, Y.-W. Son, M. L. Cohen and S. G. Louie, Quasiparticle energies and band gaps in graphene nanoribbons, *Phys. Rev. Lett.*, 2007, **99**, 186801.
22 P. Wagner, C. P. Ewels, J.-J. Adjizian, L. Magaud, P. Pochet, S. Roche, A. Lopez-Bezanilla, V. V. Ivanovskaya, A. Yaya, M. Rayson, *et al.*, Band gap engineering *via* edge-functionalization of graphene nanoribbons, *J. Phys. Chem. C*, 2013, **117**, 26790.
23 A. Mehri and M. Jamaati, Electron transport in ladder-shaped graphene cuts, *Comput. Mater. Sci.*, 2019, **158**, 265.
24 X. Yi, M. Long, A. Liu, M. Li and H. Xu, First principles study on the electronic structures and transport properties of armchair/zigzag edge hybridized graphene nanoribbons, *J. Appl. Phys.*, 2018, **123**, 204303.
25 W. Liu, F. Meng, C. Fang, J. Zhao, J. Cheng and X. Jiang, Size effect of v-shaped notches on the electronic transport properties of zigzag graphene nanoribbons, *Comput. Condens. Matter*, 2017, **10**, 10.
26 L. Du, T. N. Nguyen, A. Gilman, A. R. Muniz and D. Maroudas, Tuning the band structure of graphene nanoribbons through defect-interaction-driven edge patterning, *Phys. Rev. B: Condens. Matter Mater. Phys.*, 2017, **96**, 245422.
27 W. F. da Cunha, P. H. de Oliveira Neto, A. Terai and G. M. e Silva, Dynamics of charge carriers on hexagonal nanoribbons with vacancy defects, *Phys. Rev. B: Condens. Matter Mater. Phys.*, 2016, **94**, 014301.
28 J. F. Teixeira, P. H. de Oliveira Neto, W. F. da Cunha, L. A. Ribeiro and G. M. e Silva, Bond length pattern associated with charge carriers in armchair graphene nanoribbons, *J. Mol. Model.*, 2017, **23**, 293.
29 W. F. da Cunha, P. H. Acioli, P. H. de Oliveira Neto, R. Gargano and G. M. e Silva, Polaron properties in armchair graphene nanoribbons, *J. Phys. Chem. A*, 2016, **120**, 4893.
30 L. A. Ribeiro Jr, W. F. da Cunha, A. L. d. A. Fonseca, G. M. e Silva and S. Stafstrom, Transport of polarons in graphene nanoribbons, *J. Phys. Chem. Lett.*, 2015, **6**, 510.
31 V. N. Kotov, B. Uchoa, V. M. Pereira, F. Guinea and A. C. Neto, Electron-electron interactions in graphene: current status and perspectives, *Rev. Mod. Phys.*, 2012, **84**, 1067.
32 C. Lee, X. Wei, J. W. Kysar and J. Hone, Measurement of the elastic properties and intrinsic strength of monolayer graphene, *Science*, 2008, **321**, 385.
33 A. V. P. Abreu, J. F. Teixeira, A. L. d. A. Fonseca, R. Gargano, G. M. e Silva and L. A. Ribeiro, Impact of the electron–phonon interactions on the polaron dynamics in graphene nanoribbons, *J. Phys. Chem. A*, 2016, **120**, 4901.
34 K. Wakabayashi, Y. Takane, M. Yamamoto and M. Sigrist, Electronic transport properties of graphene nanoribbons, *New J. Phys.*, 2009, **11**, 095016.
35 A. Sarmah and P. Hobza, Understanding the spin-dependent electronic properties of symmetrically far-edge doped zigzag graphene nanoribbon from a first principles study, *RSC Adv.*, 2017, **7**, 46604.
36 J. Guo, D. Gunlycke and C. White, Field effect on spin-polarized transport in graphene nanoribbons, *Appl. Phys. Lett.*, 2008, **92**, 163109.
37 D. Gunlycke, D. A. Areshkin, J. Li, J. W. Mintmire and C. T. White, Graphene nanostrip digital memory device, *Nano Lett.*, 2007, **7**, 3608.
38 F. J. Martín-Martínez, S. Fias, G. Van Lier, F. De Proft and P. Geerlings, Electronic structure and aromaticity of graphene nanoribbons, *Chem.–Eur. J.*, 2012, **18**, 6183.
39 C.-S. Wu and J.-D. Chai, Electronic properties of zigzag graphene nanoribbons studied by tao-dft, *J. Chem. Theory Comput.*, 2015, **11**, 2003.
40 S. Osella, A. Narita, M. G. Schwab, Y. Hernandez, X. Feng, K. Mullen and D. Beljonne, Graphene nanoribbons as low band gap donor materials for organic photovoltaics: quantum chemical aided design, *ACS Nano*, 2012, **6**, 5539.
41 Y. Hu, P. Xie, M. De Corato, A. Ruini, S. Zhao, F. Meggendorfer, L. A. Straasø, L. Rondin, P. Simon, J. Li, *et al.*, Bandgap engineering of graphene nanoribbons by control over structural distortion, *J. Am. Chem. Soc.*, 2018, **140**, 7803.
42 I. Ivanov, Y. Hu, S. Osella, U. Beser, H. I. Wang, D. Beljonne, A. Narita, K. Mullen, D. Turchinovich and M. Bonn, Role of edge engineering in photoconductivity of graphene nanoribbons, *J. Am. Chem. Soc.*, 2017, **139**, 7982.
43 A. Narita, I. A. Verzhbitskiy, W. Frederickx, K. S. Mali, S. A. Jensen, M. R. Hansen, M. Bonn, S. De Feyter, C. Casiraghi, X. Feng, *et al.*, Bottom-up synthesis of liquid-phase-processable graphene nanoribbons with near-infrared absorption, *ACS Nano*, 2014, **8**, 11622.
44 W. F. da Cunha, P. H. de Oliveira Neto, L. A. R. Junior and G. M. e Silva, Quasiparticle description of transition metal dichalcogenide nanoribbons, *Phys. Rev. B*, 2019, **99**, 035405.

Bibliography

[1] Kostya S Novoselov, Andre K Geim, Sergei V Morozov, Dingde Jiang, Yanshui Zhang, Sergey V Dubonos, Irina V Grigorieva, and Alexandr A Firsov. Electric field effect in atomically thin carbon films. *science*, 306(5696):666–669, 2004.

[2] Caterina Soldano, Ather Mahmood, and Erik Dujardin. Production, properties and potential of graphene. *Carbon*, 48(8):2127–2150, 2010.

[3] Anindya Nag, Arkadeep Mitra, and Subhas Chandra Mukhopadhyay. Graphene and its sensor-based applications: A review. *Sensors and Actuators A: Physical*, 270:177–194, 2018.

[4] Minkyu Park, Sun-Chul Lee, and Yong-Sung Kim. Length-dependent lattice thermal conductivity of graphene and its macroscopic limit. *Journal of Applied Physics*, 114(5):053506, 2013.

[5] Phaedon Avouris and Fengnian Xia. Graphene applications in electronics and photonics. *Mrs Bulletin*, 37(12):1225–1234, 2012.

[6] Changgu Lee, Xiaoding Wei, Jeffrey W Kysar, and James Hone. Measurement of the elastic properties and intrinsic strength of monolayer graphene. *science*, 321(5887):385–388, 2008.

[7] Peter Blake, Paul D Brimicombe, Rahul R Nair, Tim J Booth, Da Jiang, Fred Schedin, Leonid A Ponomarenko, Sergey V Morozov, Helen F Gleeson, Ernie W Hill, et al. Graphene-based liquid crystal device. *Nano letters*, 8(6):1704–1708, 2008.

[8] Xuan Wang, Linjie Zhi, and Klaus Müllen. Transparent, conductive graphene electrodes for dye-sensitized solar cells. *Nano letters*, 8(1):323–327, 2008.

[9] Alexander A Balandin, Suchismita Ghosh, Wenzhong Bao, Irene Calizo, Desalegne Teweldebrhan, Feng Miao, and Chun Ning Lau. Superior thermal conductivity of single-layer graphene. *Nano letters*, 8(3):902–907, 2008.

[10] AH Castro Neto, Francisco Guinea, Nuno MR Peres, Kostya S Novoselov, and Andre K Geim. The electronic properties of graphene. *Reviews of modern physics*, 81(1):109, 2009.

[11] Zhen Xu and Chao Gao. Graphene fiber: a new trend in carbon fibers. *Materials Today*, 18(9):480–492, 2015.

[12] Keqing Zhou, Zhou Gui, and Yuan Hu. The influence of graphene based smoke suppression agents on reduced fire hazards of polystyrene composites. *Composites Part A: Applied Science and Manufacturing*, 80:217–227, 2016.

[13] Sergey Rumyantsev, Guanxiong Liu, Michael S Shur, Radislav A Potyrailo, and Alexander A Balandin. Selective gas sensing with a single pristine graphene transistor. *Nano letters*, 12(5):2294–2298, 2012.

[14] Congyu Wu, Xiaochen Wu, Yongqiang Yang, Xuejiao Zhou, Haixia Wu, et al. Biological applications of graphene and graphene oxide. *Nano Biomedicine & Engineering*, 4(4), 2012.

[15] Emiliano Pallecchi, Christian Benz, AC Betz, H v Löhneysen, Bernard Plaçais, and Ro-

main Danneau. Graphene microwave transistors on sapphire substrates. *Applied Physics Letters*, 99(11):113502, 2011.

[16] JS Moon, D Curtis, M Hu, D Wong, C McGuire, PM Campbell, G Jernigan, JL Tedesco, B VanMil, R Myers-Ward, et al. Epitaxial-graphene rf field-effect transistors on si-face 6h-sic substrates. *IEEE Electron Device Letters*, 30(6):650–652, 2009.

[17] Yuxuan Lin, Xinming Li, Dan Xie, Tingting Feng, Yu Chen, Rui Song, He Tian, Tianling Ren, Minlin Zhong, Kunlin Wang, et al. Graphene/semiconductor heterojunction solar cells with modulated antireflection and graphene work function. *Energy & Environmental Science*, 6(1):108–115, 2013.

[18] Hoik Lee, Keewook Paeng, and Ick Soo Kim. A review of doping modulation in graphene. *Synthetic Metals*, 244:36–47, 2018.

[19] Stefano Agnoli and Marco Favaro. Doping graphene with boron: a review of synthesis methods, physicochemical characterization, and emerging applications. *Journal of Materials Chemistry A*, 4(14):5002–5025, 2016.

[20] Rebti Bhushan, Prashant Kumar, and AK Thakur. Catalyst-free solvothermal synthesis of ultrapure elemental n-and b-doped graphene for energy storage application. *Solid State Ionics*, 353:115371, 2020.

[21] Antony R Thiruppathi, Boopathi Sidhureddy, Michael Salverda, Peter C Wood, and Aicheng Chen. Novel three-dimensional n-doped interconnected reduced graphene ox-

ide with superb capacitance for energy storage. *Journal of Electroanalytical Chemistry*, 875:113911, 2020.

[22] SK Basiruddin and Sarat K Swain. Phenylboronic acid functionalized reduced graphene oxide based fluorescence nano sensor for glucose sensing. *Materials Science and Engineering: C*, 58:103–109, 2016.

[23] Ruitao Lv, Gugang Chen, Qing Li, Amber McCreary, Andrés Botello-Méndez, SV Morozov, Liangbo Liang, Xavier Declerck, Nestor Perea-López, David A Cullen, et al. Ultrasensitive gas detection of large-area boron-doped graphene. *Proceedings of the National Academy of Sciences*, 112(47):14527–14532, 2015.

[24] Xiao Li, Lili Fan, Zhen Li, Kunlin Wang, Minlin Zhong, Jinquan Wei, Dehai Wu, and Hongwei Zhu. Boron doping of graphene for graphene–silicon p–n junction solar cells. *Advanced Energy Materials*, 2(4):425–429, 2012.

[25] Arlenciu Celis, M Narayanan Nair, Amina Taleb-Ibrahimi, EH Conrad, Claire Berger, WA De Heer, and Antonio Tejeda. Graphene nanoribbons: fabrication, properties and devices. *Journal of Physics D: Applied Physics*, 49(14):143001, 2016.

[26] Young-Woo Son, Marvin L Cohen, and Steven G Louie. Energy gaps in graphene nanoribbons. *Physical review letters*, 97(21):216803, 2006.

[27] Li Yang, Marvin L Cohen, and Steven G Louie. Excitonic effects in the optical spectra of graphene nanoribbons. *Nano letters*, 7(10):3112–3115, 2007.

[28] Li Yang, Cheol-Hwan Park, Young-Woo Son, Marvin L Cohen, and Steven G Louie. Quasiparticle energies and band gaps in graphene nanoribbons. *Physical Review Letters*, 99(18):186801, 2007.

[29] Asha P Johnson, Chinnu Sabu, N Kumara Swamy, Annstephy Anto, HV Gangadharappa, and K Pramod. Graphene nanoribbon: An emerging and efficient flat molecular platform for advanced biosensing. *Biosensors and Bioelectronics*, page 113245, 2021.

[30] Hao Bu, Yunfei Chen, Min Zou, Hong Yi, Kedong Bi, and Zhonghua Ni. Atomistic simulations of mechanical properties of graphene nanoribbons. *Physics Letters A*, 373(37):3359–3362, 2009.

[31] Akimitsu Narita, Xinliang Feng, Yenny Hernandez, Søren A Jensen, Mischa Bonn, Huafeng Yang, Ivan A Verzhbitskiy, Cinzia Casiraghi, Michael Ryan Hansen, Amelie HR Koch, et al. Synthesis of structurally well-defined and liquid-phase-processable graphene nanoribbons. *Nature chemistry*, 6(2):126, 2014.

[32] Ming-Wei Lin, Cheng Ling, Luis A Agapito, Nicholas Kioussis, Yiyang Zhang, Mark Ming-Cheng Cheng, Wei L Wang, Efthimios Kaxiras, and Zhixian Zhou. Approaching the intrinsic band gap in suspended high-mobility graphene nanoribbons. *Physical Review B*, 84(12):125411, 2011.

[33] Zhixin Guo, Dier Zhang, and Xin-Gao Gong. Thermal conductivity of graphene nanoribbons. *Applied physics letters*, 95(16):163103, 2009.

[34] Yu Zhu, Amanda L Higginbotham, and James M Tour. Covalent functionalization of

surfactant-wrapped graphene nanoribbons. *Chemistry of Materials*, 21(21):5284–5291, 2009.

[35] Yunbin Hu, Peng Xie, Marzio De Corato, Alice Ruini, Shen Zhao, Felix Meggendorfer, Lasse Arnt Straasø, Loic Rondin, Patrick Simon, Juan Li, et al. Bandgap engineering of graphene nanoribbons by control over structural distortion. *Journal of the American Chemical Society*, 140(25):7803–7809, 2018.

[36] Luiz Antonio Ribeiro Jr, Wiliam Ferreira da Cunha, Antonio Luciano de Almeida Fonseca, Geraldo Magela e Silva, and Sven Stafstrom. Transport of polarons in graphene nanoribbons. *The journal of physical chemistry letters*, 6(3):510–514, 2015.

[37] Tiago de Sousa Araújo Cassiano, Fábio Ferreira Monteiro, Leonardo Evaristo de Sousa, Geraldo Magela e Silva, and Pedro Henrique de Oliveira Neto. Smooth gap tuning strategy for cove-type graphene nanoribbons. *RSC Advances*, 10(45):26937–26943, 2020.

[38] Marcelo Lopes Pereira Júnior, Pedro Henrique de Oliveira Neto, Demétrio Antônio da Silva Filho, Leonardo Evaristo de Sousa, Geraldo Magela e Silva, and Luiz Antônio Ribeiro Júnior. Charge localization and hopping in a topologically engineered graphene nanoribbon. *Scientific Reports*, 11(1):1–9, 2021.

[39] Yea-Lee Lee, Fangzhou Zhao, Ting Cao, Jisoon Ihm, and Steven G Louie. Topological phases in cove-edged and chevron graphene nanoribbons: Geometric structures, z 2 invariants, and junction states. *Nano letters*, 18(11):7247–7253, 2018.

[40] Daniel J Rizzo, Gregory Veber, Ting Cao, Christopher Bronner, Ting Chen, Fangzhou

Zhao, Henry Rodriguez, Steven G Louie, Michael F Crommie, and Felix R Fischer. Topological band engineering of graphene nanoribbons. *Nature*, 560(7717):204, 2018.

[41] WenXing Zhang. Voltage-driven spintronic logic gates in graphene nanoribbons. *Scientific reports*, 4(1):1–5, 2014.

[42] Er-jun Kan, Zhenyu Li, Jinlong Yang, and JG Hou. Half-metallicity in edge-modified zigzag graphene nanoribbons. *Journal of the American Chemical Society*, 130(13):4224–4225, 2008.

[43] Sukhbir Singh, Abir De Sarkar, and Inderpreet Kaur. A comparative and a systematic study on the effects of b, n doping and c-atom vacancies on the band gap in narrow zig-zag graphene nanoribbons via quantum transport calculations. *Materials Research Bulletin*, 87:167–176, 2017.

[44] Akimitsu Narita, Ivan A Verzhbitskiy, Wout Frederickx, Kunal S Mali, Soeren Alkaersig Jensen, Michael Ryan Hansen, Mischa Bonn, Steven De Feyter, Cinzia Casiraghi, Xinliang Feng, et al. Bottom-up synthesis of liquid-phase-processable graphene nanoribbons with near-infrared absorption. *ACS nano*, 8(11):11622–11630, 2014.

[45] Guo Wang. Effect of edge-hydrogen passivation and saturation on the carrier mobility of armchair graphene nanoribbons. *Chemical Physics Letters*, 533:74–77, 2012.

[46] Kirill I Bolotin, K J Sikes, Zd Jiang, M Klima, G Fudenberg, J ea Hone, Ph Kim, and HL Stormer. Ultrahigh electron mobility in suspended graphene. *Solid state communications*, 146(9-10):351–355, 2008.

[47] Chenggang Tao, Liying Jiao, Oleg V Yazyev, Yen-Chia Chen, Juanjuan Feng, Xiaowei Zhang, Rodrigo B Capaz, James M Tour, Alex Zettl, Steven G Louie, et al. Spatially resolving edge states of chiral graphene nanoribbons. *Nature Physics*, 7(8):616–620, 2011.

[48] Martina Corso, Eduard Carbonell-Sanromà, and Dimas G de Oteyza. Chapter bottom-up fabrication of atomically precise graphene nanoribbons. In *On-Surface Synthesis II*. Springer Nature, 2018.

[49] Néstor Merino-Díez, Jingcheng Li, Aran Garcia-Lekue, Guillaume Vasseur, Manuel Vilas-Varela, Eduard Carbonell-Sanroma, Martina Corso, J Enrique Ortega, Diego Peña, Jose I Pascual, et al. Unraveling the electronic structure of narrow atomically precise chiral graphene nanoribbons. *The journal of physical chemistry letters*, 9(1):25–30, 2018.

[50] Lingxiu Chen, Li He, Hui Shan Wang, Haomin Wang, Shujie Tang, Chunxiao Cong, Hong Xie, Lei Li, Hui Xia, Tianxin Li, et al. Oriented graphene nanoribbons embedded in hexagonal boron nitride trenches. *Nature communications*, 8(1):1–6, 2017.

[51] Vivek Saraswat, Robert M Jacobberger, and Michael S Arnold. Materials science challenges to graphene nanoribbon electronics. *ACS nano*, 15(3):3674–3708, 2021.

[52] Chuan Liu, Bing Yao, Taige Dong, Haiguang Ma, Shaobo Zhang, Junzhuan Wang, Jun Xu, Yi Shi, Kunji Chen, Libo Gao, et al. Highly stretchable graphene nanoribbon springs by programmable nanowire lithography. *npj 2D Materials and Applications*, 3(1):1–9, 2019.

[53] Kaveh Khaliji, Sudipta Romen Biswas, Hai Hu, Xiaoxia Yang, Qing Dai, Sang-Hyun

Oh, Phaedon Avouris, and Tony Low. Plasmonic gas sensing with graphene nanoribbons. *Physical Review Applied*, 13(1):011002, 2020.

[54] Ahmad N Abbas, Gang Liu, Akimitsu Narita, Manuel Orosco, Xinliang Feng, Klaus Mullen, and Chongwu Zhou. Deposition, characterization, and thin-film-based chemical sensing of ultra-long chemically synthesized graphene nanoribbons. *Journal of the American Chemical Society*, 136(21):7555–7558, 2014.

[55] Seung JooáLee, Hyeong PiláKim, Wilson Joseáda Silva, Fabio KurtáSchneider, Abd Rashid bináMohd Yusoff, et al. An organic photovoltaic featuring graphene nanoribbons. *Chemical Communications*, 51(44):9185–9188, 2015.

[56] Silvio Osella, Akimitsu Narita, Matthias Georg Schwab, Yenny Hernandez, Xinliang Feng, Klaus Mullen, and David Beljonne. Graphene nanoribbons as low band gap donor materials for organic photovoltaics: quantum chemical aided design. *ACS nano*, 6(6):5539–5548, 2012.

[57] L Jothi, N Jayakumar, SK Jaganathan, and G Nageswaran. Ultrasensitive and selective non-enzymatic electrochemical glucose sensor based on hybrid material of graphene nanosheets/graphene nanoribbons/nickel nanoparticle. *Materials Research Bulletin*, 98:300–307, 2018.

[58] Siva Kumar Krishnan, Eric Singh, Pragya Singh, Meyya Meyyappan, and Hari Singh Nalwa. A review on graphene-based nanocomposites for electrochemical and fluorescent biosensors. *RSC advances*, 9(16):8778–8881, 2019.

[59] Qiumei Feng, Xiaolei Zhao, Yuehua Guo, Mingkai Liu, and Po Wang. Stochastic dna walker for electrochemical biosensing sensitized with gold nanocages@ graphene nanoribbons. *Biosensors and Bioelectronics*, 108:97–102, 2018.

[60] Aída Martín, Pilar Batalla, Javier Hernández-Ferrer, María Teresa Martínez, and Alberto Escarpa. Graphene oxide nanoribbon-based sensors for the simultaneous bioelectrochemical enantiomeric resolution and analysis of amino acid biomarkers. *Biosensors and Bioelectronics*, 68:163–167, 2015.

[61] Lavanya Jothi, Saravana Kumar Jaganathan, and Gomathi Nageswaran. An electrodeposited au nanoparticle/porous graphene nanoribbon composite for electrochemical detection of alpha-fetoprotein. *Materials Chemistry and Physics*, 242:122514, 2020.

[62] Asha P Johnson, HV Gangadharappa, and K Pramod. Graphene nanoribbons: A promising nanomaterial for biomedical applications. *Journal of Controlled Release*, 2020.

[63] W_P Su, JR Schrieffer, and Ao J Heeger. Solitons in polyacetylene. *Physical review letters*, 42(25):1698, 1979.

[64] W-P_ Su, JR Schrieffer, and AJ Heeger. Soliton excitations in polyacetylene. *Physical Review B*, 22(4):2099, 1980.

[65] Geraldo Magela e Silva and Akira Terai. Dynamics of solitons in polyacetylene with interchain coupling. *Physical Review B*, 47(19):12568, 1993.

[66] Geraldo Magela e Silva. Electric-field effects on the competition between polarons and bipolarons in conjugated polymers. *Physical Review B*, 61(16):10777, 2000.

[67] Anders A Johansson and Sven Stafström. Nonadiabatic simulations of polaron dynamics. *Physical Review B*, 69(23):235205, 2004.

[68] Wiliam F da Cunha, Paulo H Acioli, Pedro H de Oliveira Neto, Ricardo Gargano, and Geraldo M e Silva. Polaron properties in armchair graphene nanoribbons. *The Journal of Physical Chemistry A*, 120(27):4893–4900, 2016.

[69] Marcelo Macedo Fischer, Luiz Antonio Ribeiro Junior, Wiliam Ferreira da Cunha, Leonardo Evaristo de Sousa, Geraldo Magela e Silva, and Pedro Henrique de Oliveira Neto. Ultrafast direct generation of quasiparticles in graphene nanoribbons. *Carbon*, 158:553–558, 2020.

[70] Marcelo Macedo Fischer, Leonardo Evaristo de Sousa, Leonardo Luiz e Castro, Luiz Antonio Ribeiro, Rafael Timóteo de Sousa, Geraldo Magela e Silva, and Pedro Henrique de Oliveira Neto. Effective mass of quasiparticles in armchair graphene nanoribbons. *Scientific reports*, 9(1):1–8, 2019.

[71] Maurício Bellissimo Falleiros. *Espalhamento de pólarons em compostos de poliparafenileno*. PhD thesis, Universidade de Brasília, 2019.

[72] Pedro Henrique de Oliveira Neto. *Dinâmica de fotogeração de portadores de carga em polímeros conjugados*. PhD thesis, Universidade de Brasília, 2009.

[73] Jonathan Fernando Teixeira, Pedro Henrique de Oliveira Neto, Wiliam Ferreira da Cunha, Luiz Antonio Ribeiro, and Geraldo Magela e Silva. Bond length pattern associated

with charge carriers in armchair graphene nanoribbons. *Journal of molecular modeling*, 23(10):293, 2017.

[74] Alan J Heeger, S Kivelson, JR Schrieffer, and W-P Su. Solitons in conducting polymers. *Reviews of Modern Physics*, 60(3):781, 1988.

[75] Jun John Sakurai and Eugene D Commins. *Modern quantum mechanics, revised edition*. American Association of Physics Teachers, 1995.

[76] Matheus Paes Lima and Geraldo Magela e Silva. Dynamical evolution of polaron to bipolaron in conjugated polymers. *Physical Review B*, 74(22):224304, 2006.

[77] Wiliam Ferreira da Cunha, Pedro Henrique de Oliveira Neto, Akira Terai, and Geraldo Magela e Silva. Dynamics of charge carriers on hexagonal nanoribbons with vacancy defects. *Physical Review B*, 94(1):014301, 2016.

[78] Wiliam Ferreira da Cunha, Luiz Antonio Ribeiro Junior, Antonio Luciano de Almeida Fonseca, Ricardo Gargano, and Geraldo Magela e Silva. Impurity effects on polaron dynamics in graphene nanoribbons. *Carbon*, 91:171–177, 2015.

[79] P. H. De Oliveira Neto, J. F. Teixeira, W. F. Da Cunha, R. Gargano, and G. M. E Silva. Electron-lattice coupling in armchair graphene nanoribbons. *Journal of Physical Chemistry Letters*, 3(20):3039–3042, 2012.

[80] Marcelo Lopes Pereira Junior, Wiliam Ferreira da Cunha, Rafael Timoteo de Sousa Junior, William Ferreira Giozza, Geraldo Magela e Silva, and Luiz Antonio Ribeiro Junior.

Charge transport mechanism in chevron-graphene nanoribbons. *The Journal of Physical Chemistry C*, 124(41):22392–22398, 2020.

[81] Ana Virgínia Passos Abreu, Jonathan Fernando Teixeira, Antonio Luciano de Almeida Fonseca, Ricardo Gargano, Geraldo Magela e Silva, and Luiz Antonio Ribeiro. Impact of the electron–phonon interactions on the polaron dynamics in graphene nanoribbons. *The Journal of Physical Chemistry A*, 120(27):4901–4906, 2016.

[82] Maurício Bellissimo Falleiros and Geraldo Magela e Silva. Same charge polaron and bipolaron scattering on conducting polymers. *The Journal of Physical Chemistry A*, 123(7):1319–1327, 2019.

[83] Katsunori Wakabayashi, Yositake Takane, Masayuki Yamamoto, and Manfred Sigrist. Electronic transport properties of graphene nanoribbons. *New Journal of Physics*, 11(9):095016, 2009.

[84] Amrit Sarmah and Pavel Hobza. Understanding the spin-dependent electronic properties of symmetrically far-edge doped zigzag graphene nanoribbon from a first principles study. *RSC advances*, 7(74):46604–46614, 2017.

[85] Jing Guo, D Gunlycke, and CT White. Field effect on spin-polarized transport in graphene nanoribbons. *Applied Physics Letters*, 92(16):163109, 2008.

[86] Daniel Gunlycke, Denis A Areshkin, Junwen Li, John W Mintmire, and Carter T White. Graphene nanostrip digital memory device. *Nano letters*, 7(12):3608–3611, 2007.

[87] Chun-Shian Wu and Jeng-Da Chai. Electronic properties of zigzag graphene nanoribbons studied by tao-dft. *Journal of chemical theory and computation*, 11(5):2003–2011, 2015.

[88] Ivan Ivanov, Yunbin Hu, Silvio Osella, Uliana Beser, Hai I Wang, David Beljonne, Akimitsu Narita, Klaus Mullen, Dmitry Turchinovich, and Mischa Bonn. Role of edge engineering in photoconductivity of graphene nanoribbons. *Journal of the American Chemical Society*, 139(23):7982–7988, 2017.

[89] Wiliam Ferreira da Cunha, Pedro Henrique de Oliveira Neto, Luiz Antonio Ribeiro Junior, and Geraldo Magela e Silva. Quasiparticle description of transition metal dichalcogenide nanoribbons. *Physical Review B*, 99(3):035405, 2019.